Journal of the Mechanics and Physics of Solids 135 (2020) 103777

Contents lists available at ScienceDirect

Journal of the Mechanics and Physics of Solids

journal homepage: www.elsevier.com/locate/jmps

Visco-hyperelastic constitutive modeling of strain rate sensitive soft materials

Kshitiz Upadhyay, Ghatu Subhash*, Douglas Spearot

Department of Mechanical and Aerospace Engineering, University of Florida, Gainesville, FL 32611, United States

ARTICLE INFO

Article history:
Received 13 June 2019
Revised 9 October 2019
Accepted 1 November 2019
Available online 4 November 2019

Keywords:
Constitutive modeling
Viscous dissipation potential
Large deformations
Strain rate sensitivity
Brain tissue mechanics
Hyperelasticity

ABSTRACT

A novel viscous dissipation potential is proposed for the visco-hyperelastic constitutive modeling of short-time memory responses of soft materials, which can capture both linear and nonlinear large deformation behaviors over a wide range of strain rates. The proposed potential is compatible with objectivity and continuum thermodynamics principles, consists of physically motivated model parameters, and adds the capability of modeling strain rate sensitivity in the small strain regime, which is currently not possible with available external state variable driven viscous dissipation potentials. By combining the proposed viscous dissipation potential with the Mooney-Rivlin strain energy density function, a visco-hyperelastic relation is formulated and fit to the rate-dependent tensile stress-strain data of human patellar tendon, which was previously modeled using an existing viscous dissipation potential. It is demonstrated that the proposed model offers improvements in fitting accuracy and prevents possible thermodynamic instabilities in quasi-static hyperelastic models from corrupting the dynamic response. In addition, the uncomplicated mathematical form of the model and the accompanying multi-step multi-start optimization procedure helps prevent numerical instabilities. Multi-deformation mode fitting of human brain gray matter under all three primary deformation modes (compression, tension and shear) is also considered using a visco-hyperelastic model based on the proposed potential and the semi-empirical Gent-Gent strain energy density function. It is shown that visco-hyperelastic models based on the proposed viscous dissipation potential capture all the essential features of the stress-strain data with unique optimal model parameters, giving reasonable accuracy in both single and multiple deformation mode cases. Further, it is demonstrated that the proposed model is stable and robust with respect to both the choice of the hyperelastic strain energy density and the availability of data from multiple deformation modes.

1. Introduction

The mechanical response of rubber-like polymers and many biological tissues involves large deformation, nonlinear stress-strain behavior, and time-dependence. The first two of these features (large and nonlinear deformations) have been extensively studied using hyperelasticity theory, which assumes the existence of a strain energy density function that depends on the instantaneous deformation with respect to some reference state. Accordingly, many empirical (e.g., the

* Corresponding author.
E-mail address: subhash@ufl.edu (G. Subhash).

https://doi.org/10.1016/j.jmps.2019.103777
0022-5096/

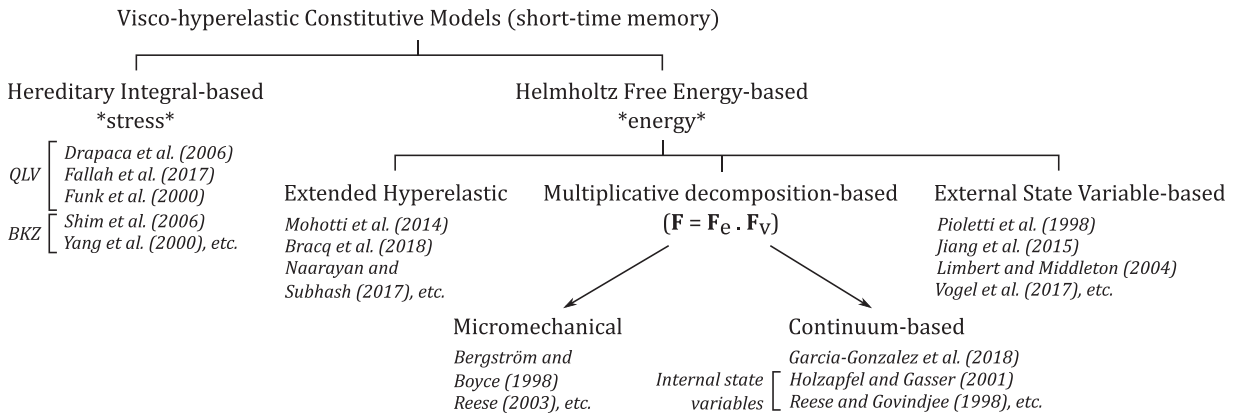

Fig. 1. Different types of short-time memory visco-hyperelastic constitutive models (with examples of each type).

Mooney-Rivlin model (Mooney, 1940; Rivlin, 1948a) and the Ogden model (Ogden, 1972)) and semi-empirical multiscale (e.g., the Arruda-Boyce model (Arruda and Boyce, 1993) and the Gent model (Gent, 1996)) constitutive models have been proposed. These models have been implemented to capture quasi-static mechanical behavior of soft materials such as rubbers (Khajehsaeid et al., 2013; Marckmann and Verron, 2006; Sasso et al., 2008), biological tissues (Avril, 2017; Naini et al., 2011; Zhong and Peters, 2007), and hydrogels (Pavan et al., 2010; Sasson et al., 2012; Zhao et al., 2015). Time-dependence, on the other hand, is a more complex phenomenon that can be broadly divided into long and short-term responses (Pioletti and Rakotomanana, 2000) based on the relative time-scales of experimental observation and equilibration of microstructure following a deformation. The long-term response includes stress relaxation and creep, as the observation time is very large compared to the time it takes for the internal microstructure to rearrange or react to the loading. Short-term responses include rate-dependent stiffening or softening of soft polymers, which are phenomena of special importance in the design of protective equipment (Payne et al., 2015), study of extreme events such as ballistic impact (Roberts et al., 2007), automobile crashes (Parnaik et al., 2004), blast (Jennifer et al., 2001), and medical conditions such as whiplash and traumatic brain injuries (Doorly and Gilchrist, 2006; Harrigan et al., 2010). The present work concerns itself with the visco-hyperelastic constitutive modeling of short-term time-dependent (also called short-time), large and nonlinear deformations of isotropic soft polymers and biological tissues.

Constitutive modeling of the short-time response of soft materials has been conducted via two broad approaches: (i) hereditary integral based models, and (ii) Helmholtz free energy based models (tree chart shown in Fig. 1). Hereditary integral based models are stress-based formulations that describe stress at a given time as a combination of elastic and viscoelastic responses, the latter being modeled as a fading-memory convolution integral involving relaxation functions to reflect the deformation history. This approach has been extensively used for rubbers and soft tissues, mainly using quasi-linear viscoelastic (QLV) models (e.g., Drapaca et al., 2006; Fallah et al., 2017a; Funk et al., 2000), and nonlinear finite viscoelastic models such as the Bernstein–Kearsley–Zapas (BKZ) models (e.g., Shim et al., 2004; Yang et al., 2000). Although applicable for a wide range of materials, these models often involve a large number of model parameters for the Prony series formulation of the relaxation function, and are phenomenological in nature (Fallah et al., 2017b).

Helmholtz free energy based models originate from thermodynamic potentials, and can be broadly divided into (i) extended hyperelastic models, (ii) models based on multiplicative decomposition of the deformation gradient, and (iii) external state variable driven viscous dissipation-based models. Extended hyperelastic models are based on a standard hyperelastic strain energy density function, to which either a strain rate based term is introduced to induce rate-sensitivity (e.g., Mohotti et al. (2014)), or the model constants are computed at individual strain rates (e.g., Bracq et al. (2018) and Naarayan and Subhash (2017)). Such models, however, are purely phenomenological and do not account for entropy production under non-equilibrium deformation, thus conflicting with the principles of thermodynamics.

Models based on the multiplicative decomposition of the deformation gradient into elastic and viscoelastic parts have been proposed via micromechanical or continuum-based approaches (Khajehsaeid et al., 2014). The former approach assumes that the viscous behavior of a material is due to a certain micromechanism (e.g., reptation of the elastically inactive network in the Bergstrom-Boyce model (Bergström and Boyce, 2000, 1998), and chain breakage and reformation in the Reese model (Reese, 2003)), which evolves according to a flow rule. Although this approach connects the mechanics to microstructural information, it can be complex and particularly challenging for modeling biological tissues for which the mechanisms associated with viscous effects are far from being fully understood (Vogel et al., 2017). For these materials, the microstructure, composition, and/or the viscous mechanisms can differ significantly from one to another, and so the “micromechanical” model parameters may not have any clear meaning (Xiang et al., 2019). Continuum-based approaches do not consider the underlying microstructure of the material; examples include models proposed by Garcia-Gonzalez et al. (2018), Holzapfel and Gasser (2001) and Reese and Govindjee (1998). The latter two models are based on the framework of Simo (1987), and split the Helmholtz free energy into equilibrium and non-equilibrium components, the

latter described using a set of internal state variables. These type of models have been used to describe viscoelastic and viscoplastic deformation of polymers (Amin et al., 2006; Laiarinandrasana et al., 2003) and soft tissues (Haldar and Pal, 2018), but require introduction of a number of internal variables that a priori lack any physical meaning. Note that many of the models that are based on multiplicative decomposition of deformation gradient also result in a convolution (or hereditary) integral-based stress equation.

The final class of short-time memory visco-hyperelastic models use external thermodynamic state variables to relate the strain rate stiffening or softening of material response to the irreversible thermodynamic processes arising via the evolution of internal microstructure at high strain rates. First proposed by Pioletti et al. (1998), these models assume that the entropy production under non-equilibrium strain rates occurs entirely due to viscous dissipation, which in turn is modeled using the objective strain rate tensor as an external state variable. In addition to physically based external state variables, these models feature many benefits: (i) compatibility with the principles of thermodynamics and objectivity, (ii) easy identification of model constants, (iii) convenient finite element (FE) implementation, and (iv) the ability to capture large nonlinear deformations and strain rate dependency of both isotropic and anisotropic materials. Consequently, these models have been implemented on numerous soft tissues, including ligaments and tendons (Jiang et al., 2015; Limbert and Middleton, 2004; Pioletti et al., 1998; Zhurov et al., 2007), skeletal muscles (Lu et al., 2010), annulus fibrosus (Vogel et al., 2017), tongue tissue (Yousefi et al., 2018), and brain and pericardium (Kulkarni et al., 2016). The present study considers the external state variable-based approach for the visco-hyperelastic modeling of soft materials (henceforth, viscous dissipation potential in this manuscript by-default means it is a function of external state variables).

External state variable driven viscous dissipation-based visco-hyperelastic models (Pioletti et al., 1998) generally employ an additive relationship between the hyperelastic nominal stress $\mathbf{T}_h^0$ under quasi-static equilibrium and the viscous overstress $\mathbf{T}_v^0$ under high strain rate

$$\mathbf{T}^0 = \mathbf{T}_h^0 + \mathbf{T}_v^0 \tag{1}$$

where $\mathbf{T}_h^0$ and $\mathbf{T}_v^0$ are obtained by taking derivatives of the hyperelastic strain energy density function $W_h(\mathbf{C})$ and the viscous dissipation potential $W_v(\mathbf{C}, \dot{\mathbf{C}})$ with respect to the right Cauchy-Green deformation tensor $\mathbf{C}$ and its time derivative $\dot{\mathbf{C}}$, respectively. Note that $\dot{\mathbf{C}}$ is the external thermodynamic state variable that is used to describe viscous dissipation effects. W_h can be selected from a number of invariant or principal stretch-based hyperelastic strain energy density forms available in the literature. On the other hand, W_v is expressed in terms of scalar invariants (Boehler, 1987); all existing viscous dissipation potentials for isotropic solids currently in the literature follow a general form

$$W_v = W_v(I_1, J_2) = \eta (I_1 - 3)^{\beta} J_2 \tag{2}$$

where $I_1 = \mathrm{tr}(\mathbf{C})$ is the first invariant of the right Cauchy-Green deformation tensor $\mathbf{C}$, $J_2 = \mathrm{tr}(\dot{\mathbf{C}}^2)$, and η and β are model parameters.

One major limitation of the form in Eq. (2) is that since it is purely phenomenological, the individual model parameters do not connect the macroscopic deformation to any physical or micromechanical property (Pioletti, 2006). In addition, as will be mathematically proven in Section 2, the small strain uniaxial and shear moduli resulting from a visco-hyperelastic model based on Eq. (2) are independent of the applied strain rate. This directly conflicts with experimental evidence on soft polymers and biological tissues (Arbogast and Margulies, 1998; Hrapko et al., 2006; Kwon and Subhash, 2010; Siviour and Jordan, 2016; Upadhyay et al., 2019a), many of which exhibit significant strain rate-sensitivity. Furthermore, although these models have been demonstrated to capture accurately a single primary deformation mode (compression, tension, or shear) at different strain rates, no attempt has been made to fit combined experimental data from multiple deformation modes. This is a particularly concerning issue because model parameters obtained from one deformation can yield poor results for another deformation mode or for a complex tri-axial deformation (Ogden et al., 2004), and consideration of all three primary deformation modes is usually recommended (Ogden, 1972; Upadhyay et al., 2019b). It remains to be investigated how and if these short-time visco-hyperelastic models can capture multiple deformation modes without the addition of an excessive number of viscoelastic model parameters.

In this study, a novel generalized form of the viscous dissipation potential is proposed, which not only has physically motivated model parameters, but also captures the strain rate sensitivity of mechanical response under simultaneous multiple primary deformation modes. Thus, the proposed form is a significant advancement over existing forms that follow Eq. (2). In Section 2, the continuum mechanical basis for a general viscous dissipation based visco-hyperelastic relation is presented. In addition, the rate-insensitivity of elastic moduli yielded by the existing form in Eq. (2) is demonstrated, which is a major motivation for the present work. In Section 3, a generalized rate-sensitive viscous dissipation potential is introduced, which leads to a particular three-parameter form investigated in this study, consisting of separate linear and nonlinear rate-sensitivity parts. In Section 4, the proposed viscous dissipation potential is combined with the Mooney-Rivlin strain energy density function to formulate a visco-hyperelastic model, which is applied to capture the rate-dependent uniaxial tension response of human patellar tendon (Pioletti et al., 1998). The obtained fitting accuracy and thermodynamic stability are compared against those resulting from the use of an existing viscous dissipation potential of the form of Eq. (2). Multi-deformation modeling is considered in Section 5, where a visco-hyperelastic model based on the quasi-static Gent-Gent strain energy density (Pucci and Saccomandi, 2002) and the proposed viscous dissipation potential is used to fit the combined compression-tension-shear data of human brain gray matter (Jin et al., 2013). The robustness of a visco-hyperelastic model based on the proposed viscous dissipation potential is investigated in Section 6 both with respect to the choice of

the hyperelastic strain energy density function and the availability of data from different deformation modes. Two additional single deformation mode applications (uniaxial compression of ballistic gelatin and simple shear of porcine brain) are provided in Appendix A to highlight the versatility of the proposed model under various types of loading conditions and for different material systems. Finally, the details of curve fitting/optimization, sensitivity analysis, and thermodynamic stability analysis are provided in the supplementary material.

2. Theory and background

2.1. External state variable driven viscous dissipation-based visco-hyperelastic constitutive modeling

The reference configuration local forms of the conservation of energy and Clausius-Duhem entropy inequality in continuum mechanics are

$$\rho_0 \dot{u}_0 = \mathbf{T}^0 \cdot\cdot \dot{\mathbf{F}} - \nabla_0 \cdot \mathbf{Q} + \rho_0 R \tag{3}$$

$$\rho_0 \dot{\eta}_0 + \nabla_0 \cdot \left(\frac{\mathbf{Q}}{\theta}\right) - \rho_0 \frac{R}{\theta} \geq 0 \tag{4}$$

where ρ_0 is the mass density, u_0 is the specific internal energy, $\mathbf{T}^0$ is the nominal stress tensor, $\mathbf{F}$ is the deformation gradient tensor, $\mathbf{Q}$ is the heat flux, R is the rate of internal heating per unit mass, η_0 is the specific entropy, and θ is the absolute temperature. Note that subscript 0 represents the reference system configuration, and the symbol $\cdot\cdot$ defines an alternative definition of tensor scalar product (Malvern, 1969), such that $\mathbf{T}^0 \cdot\cdot \dot{\mathbf{F}} = T^0_{ij}\dot{F}_{ji}$ in rectangular Cartesians. By substituting R from Eq. (3) into Eq. (4), and introducing the Helmholtz free energy function, $\psi = u_0 - \theta\eta_0$,

$$\mathbf{T}^0 \cdot\cdot \dot{\mathbf{F}} - \rho_0\left(\dot{\psi} + \dot{\theta}\eta_0\right) - \frac{\mathbf{Q}}{\theta}(\nabla_0 \cdot \theta) \geq 0 \tag{5}$$

Assuming isothermal deformation,

$$\Xi_{int} = \mathbf{T}^0 \cdot\cdot \dot{\mathbf{F}} - \rho_0 \dot{\psi} \geq 0 \tag{6}$$

where Ξ_{int} is the local entropy production or internal dissipation (Limbert and Middleton, 2004). For an ideal hyperelastic material, the Helmholtz free energy function depends only on the current deformed configuration, such that $\psi = \psi(\mathbf{F}, \theta)$. Such a material under quasi-static (equilibrium) isothermal deformation undergoes zero dissipation, i.e.,

$$\Xi_{int} = \left(\mathbf{T}^{0^{\mathrm{T}}} - \rho_0 \frac{\partial \psi}{\partial \mathbf{F}}\right) : \dot{\mathbf{F}} = 0 \;\Rightarrow \mathbf{T}^{0^{\mathrm{T}}} = \rho_0 \frac{\partial \psi}{\partial \mathbf{F}} = \frac{\partial W_h(\mathbf{F})}{\partial \mathbf{F}} \tag{7}$$

where $W_h(\mathbf{F})$ is the hyperelastic strain energy density function. In terms of the objective right Cauchy-Green deformation tensor $\mathbf{C} = \mathbf{F}^{\mathrm{T}} \cdot \mathbf{F}$,

$$\mathbf{T}^{0^{\mathrm{T}}} = 2\mathbf{F} \cdot \frac{\partial W_h(\mathbf{C})}{\partial \mathbf{C}} \tag{8}$$

$W_h(\mathbf{C})$ is generally defined in terms of the scalar invariants of $\mathbf{C}$ as

$$W_h = W_h(\mathbf{C}) = W_h(I_1, I_2, I_3) \tag{9}$$

where

$$I_1 = \mathrm{tr}(\mathbf{C});\; I_2 = \frac{1}{2}\left[(I_1)^2 - \mathrm{tr}\left(\mathbf{C}^2\right)\right];\; I_3 = \det(\mathbf{C}) \tag{10}$$

Eq. (7) holds for many biomaterials and polymers in rubbery state under quasi-static deformation. However, material response may deviate from this ideal behavior under high strain rates. For example, the reptational motion of a secondary polymer network, which is loosely connected to the primary load bearing polymer network, is a typical phenomenon associated with time-dependence in the mechanical behavior of elastomers (Bergström and Boyce, 2000, 1998). In biological materials, on the other hand, this time-dependent behavior has been attributed to interstitial fluid flow (Mak, 1986), tissue phase viscous interactions (Vogel et al., 2017), inherent viscoelasticity of fibers and extracellular matrix (Svensson et al., 2010), and the various biological processes causing the exchange of mass and energy between a cell and its surroundings. Regardless of the actual mechanism causing viscous effects, it is assumed that for a short-time memory response, the internal dissipation can be derived from a viscous dissipation potential function $W_v = W_v(\mathbf{C}^{(n)}),\; n = 0, 1, 2\ldots.$

$$\Xi_{int} = \left(2\mathbf{F} \cdot \frac{\partial W_v\left(\mathbf{C}^{(n)}\right)}{\partial \dot{\mathbf{C}}}\right) : \dot{\mathbf{F}} = \left(\mathbf{T}^{0^{\mathrm{T}}} - 2\mathbf{F} \cdot \frac{\partial W_h(\mathbf{C})}{\partial \mathbf{C}}\right) : \dot{\mathbf{F}} \geq 0 \tag{11}$$

where superscript (n) denotes the n^{th} derivative of $\mathbf{C}$, which is related to the frame-indifferent Rivlin-Ericksen tensor $\mathbf{A}^{(n)}$ (Malvern, 1969) as

$$\mathbf{C}^{(n)} = \mathbf{F}^{\mathrm{T}} \cdot \mathbf{A}^{(n)} \cdot \mathbf{F} \tag{12}$$

Further, assuming the viscous dissipation potential depends on only the first two derivatives ($n=0$ and 1) of $\mathbf{C}$, using the irreducible integrity basis for the polynomial scalar invariants of tensors $\mathbf{C}$ and $\dot{\mathbf{C}}$ (Malvern, 1969),

$$W_v = W_v\left(\mathbf{C}, \dot{\mathbf{C}}\right) = W_v(I_1, I_2, I_3, J_1, J_2, J_3, J_4, J_5, J_6, J_7) \tag{13}$$

where

$$\begin{aligned} &J_1 = \mathrm{tr}\left(\dot{\mathbf{C}}\right);\ J_2 = \mathrm{tr}\left(\dot{\mathbf{C}}^2\right);\ J_3 = \mathrm{tr}\left(\dot{\mathbf{C}}^3\right); \\ &J_4 = \mathrm{tr}\left(\mathbf{C}\dot{\mathbf{C}}\right);\ J_5 = \mathrm{tr}\left(\mathbf{C}\dot{\mathbf{C}}^2\right);\ J_6 = \mathrm{tr}\left(\mathbf{C}^2\dot{\mathbf{C}}\right);\ J_7 = \mathrm{tr}\left(\mathbf{C}^2\dot{\mathbf{C}}^2\right) \end{aligned} \tag{14}$$

Finally, Eq. (11) yields the visco-hyperelastic additive relationship between the hyperelastic stress and viscous overstress tensor components for the nominal ($\mathbf{T}^0$) and Cauchy stress ($\boldsymbol{\sigma}$) tensors

$$\mathbf{T}^{0^{\mathrm{T}}} = \mathbf{T}^{0^{\mathrm{T}}}_h + \mathbf{T}^{0^{\mathrm{T}}}_v = 2\mathbf{F}\cdot\frac{\partial}{\partial\mathbf{C}}W_h(I_1, I_2, I_3) + 2\mathbf{F}\cdot\frac{\partial}{\partial\dot{\mathbf{C}}}W_v(I_1, I_2, I_3, J_1, J_2, J_3, J_4, J_5, J_6, J_7) \tag{15a}$$

$$\boldsymbol{\sigma} = \boldsymbol{\sigma}_h + \boldsymbol{\sigma}_v = \frac{2}{det\,(\mathbf{F})}\mathbf{F}\cdot\left(\frac{\partial}{\partial\mathbf{C}}W_h(I_1, I_2, I_3) + \frac{\partial}{\partial\dot{\mathbf{C}}}W_v(I_1, I_2, I_3, J_1, J_2, J_3, J_4, J_5, J_6, J_7)\right)\cdot\mathbf{F}^{\mathrm{T}} \tag{15b}$$

where subscripts h and v represent individual hyperelastic and viscous overstress contributions, respectively. Note that the visco-hyperelastic relations in Eqs. (15a) and (15b) only consider derivatives of $\mathbf{C}$ in the current configuration, which depend on the immediate deformation history and not the entire deformation event; thus, the present formulation is only valid when deviation from hyperelastic behavior is due to short-term memory effects.

2.2. Motivation

Since first proposed by Pioletti et al. (1998), the viscous dissipation potential function has been used in many studies (Jiang et al., 2015; Kulkarni et al., 2016; Limbert and Middleton, 2004; Lu et al., 2010; Pioletti and Rakotomanana, 2000; Yousefi et al., 2018), all sharing a common form for isotropic deformation given in Eq. (2) and restated here for convenience

$$W_v = W_v(I_1, J_2) = \eta(I_1 - 3)^{\beta}J_2 \tag{2}$$

Most commonly, β is taken as unity. It can be verified that for a visco-hyperelastic model of the form in Eq. (15) assuming incompressibility ($I_3 = 1$), by using arbitrary hyperelastic strain energy density forms W_h (I_1, I_2) and Eq. (2) as the viscous dissipation potential, the Cauchy stress tensor (Eq. (15b)) becomes

$$\boldsymbol{\sigma} = -p\mathbf{1} + s_1\mathbf{B} + s_{-1}\mathbf{B}^{-1} + h_{\mathrm{D}}\mathbf{B}\cdot\mathbf{D}\cdot\mathbf{B} \tag{16}$$

where p is the indeterminate Lagrange multiplier for incompressibility constraint, $\mathbf{1}$ is the unit symmetric tensor, $\mathbf{B}$ is the left Cauchy-Green deformation tensor ($\mathbf{B} = \mathbf{F}\cdot\mathbf{F}^{\mathrm{T}}$), $\mathbf{D}$ is the rate of deformation tensor ($\mathbf{D} = \mathrm{sym}(\dot{\mathbf{F}}\cdot\mathbf{F}^{-1})$), and s_1, s_{-1}, and h_{D} are response functions, which depend on both model constants and the current values of strain and strain rate. Note that Eqs. (15b) and (16) are equivalent forms, and that while s_1 and s_{-1} are standard hyperelastic response functions that define the quasi-static response, h_{D} is the viscoelastic response function that defines the rate-dependent material response.

Although it is uncomplicated and amicable with FE modeling, Eq. (2) has several major drawbacks. In addition to the model parameters being purely phenomenological in nature, this form does not capture the strain rate dependence of elastic moduli as observed in many soft materials. This fact can be explained using continuum mechanical analysis of primary deformation modes of isotropic materials (compression, tension and shear), and will now be demonstrated for an incompressible visco-hyperelastic solid.

Consider an arbitrary invariant-based hyperelastic strain energy density function

$$W_h = W_h(I_1, I_2) \tag{17}$$

By substituting Eqs. (17) and (2) in the visco-hyperelastic Cauchy stress in Eq. (15b),

$$\boldsymbol{\sigma} = -p\mathbf{1} + 2\frac{\partial W_h}{\partial I_1}\mathbf{B} - 2\frac{\partial W_h}{\partial I_2}\mathbf{B}^{-1} + 8\eta(I_1 - 3)^{\beta}\mathbf{B}\cdot\mathbf{D}\cdot\mathbf{B} \tag{18}$$

Note, to ensure that $\boldsymbol{\sigma}(\mathbf{B} = \mathbf{1}) = 0, \beta > 0$ must hold. Comparing Eqs. (18) and (16), the various response functions are obtained as

$$s_1 = 2\frac{\partial W_h}{\partial I_1} \tag{19a}$$

$$s_{-1} = -2\frac{\partial W_h}{\partial I_2} \tag{19b}$$

$$h_{\mathrm{D}} = 8\eta(I_1 - 3)^{\beta} \tag{19c}$$

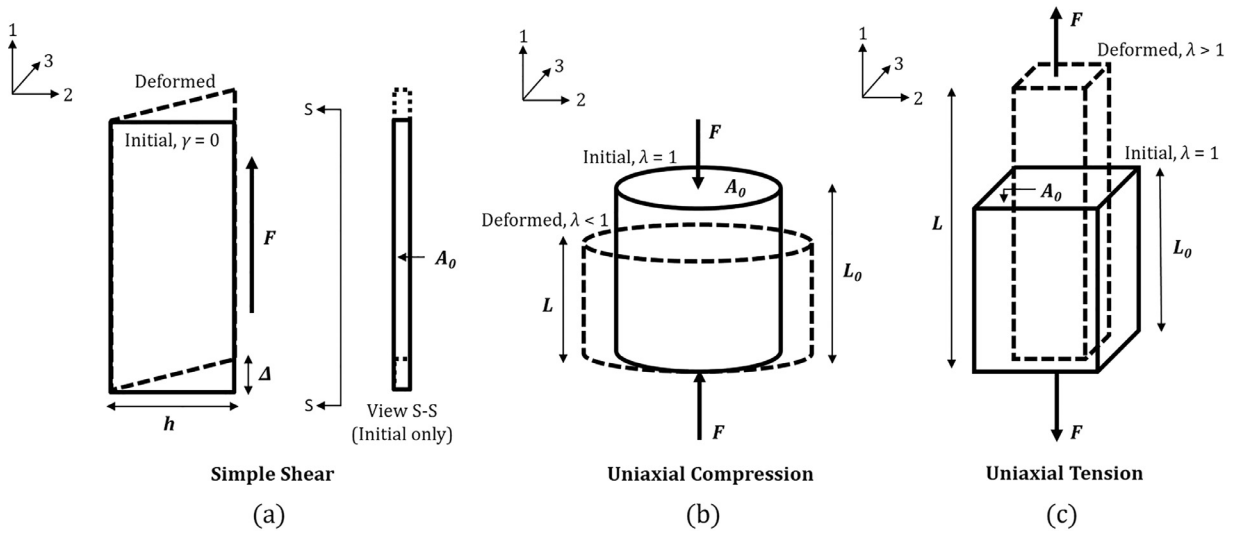

Fig. 2. Illustration of the (a) simple shear, (b) uniaxial compression and (c) uniaxial tension deformation states.

For a homogeneous simple shear deformation mode as shown in Fig. 2(a), the deformation gradient tensor is written as

$$\mathbf{F} = \begin{bmatrix} 1 & \gamma & 0 \\ 0 & 1 & 0 \\ 0 & 0 & 1 \end{bmatrix}, \ \gamma = \frac{\Delta}{h} \tag{20}$$

where γ is the nominal shear strain. Using Eq. (20), deformation tensors $\mathbf{B}$ and $\mathbf{C}$, rates $\dot{\mathbf{C}}$ and $\mathbf{D}$, and the relevant principal invariants are calculated as

$$\mathbf{B} = \begin{bmatrix} \gamma^2+1 & \gamma & 0 \\ \gamma & 1 & 0 \\ 0 & 0 & 1 \end{bmatrix}, \ \mathbf{C} = \begin{bmatrix} 1 & \gamma & 0 \\ \gamma & \gamma^2+1 & 0 \\ 0 & 0 & 1 \end{bmatrix}, \ I_1 = \gamma^2 + 3 \tag{21a}$$

$$\mathbf{D} = \frac{\dot{\gamma}}{2}\begin{bmatrix} 0 & 1 & 0 \\ 1 & 0 & 0 \\ 0 & 0 & 0 \end{bmatrix}, \ \dot{\mathbf{C}} = \dot{\gamma}\begin{bmatrix} 0 & 1 & 0 \\ 1 & 2\gamma & 0 \\ 0 & 0 & 0 \end{bmatrix}, \ J_2 = 2\dot{\gamma}^2\left(2\gamma^2+1\right) \tag{21b}$$

Tensors and invariants from Eq. (21) are used to formulate the Cauchy stress tensor $\boldsymbol{\sigma}$ in Eq. (18). Further, the condition $\mathrm{tr}\ \sigma = 0$ can be used to obtain the indeterminate Lagrange multiplier p; transforming the so obtained $\boldsymbol{\sigma}$ to the reference undeformed configuration gives the nominal shear stress as

$$T^0_{21} = 2\left(\frac{\partial W_h}{\partial I_1} + \frac{\partial W_h}{\partial I_2}\right)\gamma + 4\eta\dot{\gamma}\gamma^{2\beta}\left(1+2\gamma^2\right) \tag{22}$$

Differentiating with respect to γ and taking limit at $\gamma \to 0$, the shear modulus G_0 is obtained as

$$G_0 = \begin{cases} \infty, \ \beta \in \left(0, \frac{1}{2}\right) \\ G_{0,h} + 4\eta\dot{\gamma}, \ \beta = \frac{1}{2} \\ G_{0,h}, \ \beta \in \left(\frac{1}{2}, \infty\right) \end{cases} \tag{23}$$

where $G_{0,h}$ is the purely hyperelastic contribution to the shear modulus ($G_{0,h} = [\frac{d}{d\gamma}(2(\frac{\partial W_h}{\partial I_1} + \frac{\partial W_h}{\partial I_2})\gamma)]_{\gamma\to 0}$). Eq. (23) shows that for a single value of $\beta = 1/2$, the viscous dissipation potential form in Eq. (2) results in a strict linear rate dependence of shear modulus; otherwise, for any other value of β, a rate-independent modulus is obtained. While the former case is too stringent for a general material, the latter does not capture the well-established rate-dependence of elastic moduli observed in many soft polymers.

A similar result is also obtained for the other two primary deformation modes, uniaxial compression (Fig. 2(b)) and tension (Fig. 2(c)). In this case, the deformation gradient tensor relating the reference configuration to the deformed one is given by

$$\mathbf{F} = \begin{bmatrix} \lambda & 0 & 0 \\ 0 & \frac{1}{\sqrt{\lambda}} & 0 \\ 0 & 0 & \frac{1}{\sqrt{\lambda}} \end{bmatrix}, \ \lambda = \frac{L}{L_0} \tag{24}$$

where λ is the principal stretch ($\lambda = L/L_0$) in the $\mathbf{e}_1$ direction (standard basis $\{\mathbf{e}_1, \mathbf{e}_2, \mathbf{e}_3\}$). Using Eq. (24), the deformation tensors $\mathbf{B}$ and $\mathbf{C}$, rates $\dot{\mathbf{C}}$ and $\mathbf{D}$, and the relevant principal invariants are calculated as

$$\mathbf{B} = \mathbf{C} = \begin{bmatrix} \lambda^2 & 0 & 0 \\ 0 & \frac{1}{\lambda} & 0 \\ 0 & 0 & \frac{1}{\lambda} \end{bmatrix}, \; I_1 = \lambda^2 + \frac{2}{\lambda} \tag{25a}$$

$$\mathbf{D} = \frac{\dot{\lambda}}{\lambda}\begin{bmatrix} 1 & 0 & 0 \\ 0 & -\frac{1}{2} & 0 \\ 0 & 0 & -\frac{1}{2} \end{bmatrix}, \; \dot{\mathbf{C}} = \dot{\lambda}\begin{bmatrix} 2\lambda & 0 & 0 \\ 0 & -\frac{1}{\lambda^2} & 0 \\ 0 & 0 & -\frac{1}{\lambda^2} \end{bmatrix}, \; J_2 = 2\dot{\lambda}^2\left(2\lambda^2 + \frac{1}{\lambda^4}\right) \tag{25b}$$

Substituting tensors and invariants from Eq. (25) in Eq. (18) yields the Cauchy stress tensor $\boldsymbol{\sigma}$. By imposing the condition $\sigma_{22} = \sigma_{33} = 0$ to compute the Lagrange multiplier p, and transforming into the reference configuration, the nominal uniaxial stress is calculated as

$$T_{11}^0 = 2\frac{\partial W_h}{\partial I_1}\left(\lambda - \frac{1}{\lambda^2}\right) + 2\frac{\partial W_h}{\partial I_2}\left(1 - \frac{1}{\lambda^3}\right) + 4\eta\dot{\lambda}\left(\lambda^2 + \frac{2}{\lambda} - 3\right)^{\beta}\left(2\lambda^2 + \frac{1}{\lambda^4}\right) \tag{26}$$

Further, the uniaxial elastic modulus E_0 is obtained by differentiating Eq. (26) with respect to stretch λ, and taking limit at $\lambda \to 1$,

$$E_0 = \begin{cases} \infty, \; \beta \in \left(0, \frac{1}{2}\right) \\ E_{0,h} + 12\sqrt{3}\eta\left|\dot{\lambda}\right|, \; \beta = \frac{1}{2} \\ E_{0,h}, \; \beta \in \left(\frac{1}{2}, \infty\right) \end{cases} \tag{27}$$

where $E_{0,\,h}$ is the ideally hyperelastic contribution ($E_{0,h} = [\frac{d}{d\lambda}(2(\frac{\partial W_h}{\partial I_1}(\lambda - \frac{1}{\lambda^2}) + \frac{\partial W_h}{\partial I_2}(1 - \frac{1}{\lambda^3})))]_{\lambda \to 1}$). Again, the viscous dissipation potential form in Eq. (2) does not capture strain rate sensitivity of uniaxial elastic modulus for all but a single value of $\beta = 1/2$, when it imposes a strict linear dependence of modulus with strain rate.

Note, while the Young's modulus under quasi-static deformation is always three times the shear modulus as expected for incompressible materials, at high strain rates, Eqs. (23) and (27) with $\beta = 1/2$ cause a change in this ratio. This also changes the Poisson's ratio ν, which is related to the ratio of uniaxial and shear moduli as $\nu = ((E_0/2G_0) - 1)$. Although experimentally observed in several studies, there is no evidence that the uniaxial to shear modulus ratio changes in the dynamic regime by a fixed factor ($3\sqrt{3}$ in this case). In summary, the isotropic viscous dissipation potentials currently available in the literature (i) do not capture strain rate dependence of the elastic moduli except for one specific model parameter value, (ii) can only describe a specific linear relationship between moduli and strain rate, and (iii) require Poisson's ratio to necessarily change by a fixed factor.

3. A new viscous dissipation potential

In this section, a novel generalized form of the viscous dissipation potential is proposed to allow flexible modeling of the strain rate sensitive behavior of soft materials using physically meaningful model parameters. A specific three-parameter form is defined for further investigation in the later sections.

3.1. Generalized functional form

The following reduced form of the viscous dissipation potential (Eq. (13)) is considered in this study:

$$W_v = W_v(I_1, I_2, J_2, J_5) \tag{28}$$

Note that in addition to the invariant $J_2 = \mathrm{tr}(\dot{\mathbf{C}}^2)$ used in Eq. (2), which captures the effect of strain rate on stress, another invariant $J_5 = \mathrm{tr}(\mathbf{C}\cdot\dot{\mathbf{C}}^2)$ is added in the present formulation to include the effects of the interaction between $\mathbf{C}$ and $\dot{\mathbf{C}}$ on the viscous dissipation and stress. To justify this, consider an incompressible visco-hyperelastic solid whose strain energy density and viscous dissipation potentials are given by Eqs. (17) and (28), respectively. Computing the Cauchy overstress $\boldsymbol{\sigma}_v$ from Eq. (15b) and transforming to the symmetric second Piola-Kirchhoff overstress tensor $\mathbf{S}_v$ ($\boldsymbol{\sigma}_v = \mathbf{F}\cdot\mathbf{S}_v\cdot\mathbf{F}^{\mathrm{T}}$),

$$\mathbf{S}_v = 4\frac{\partial W_v}{\partial J_2}\dot{\mathbf{C}} + 2\frac{\partial W_v}{\partial J_5}\left(\mathbf{C}\cdot\dot{\mathbf{C}} + \dot{\mathbf{C}}\cdot\mathbf{C}\right) \tag{29}$$

From Eq. (29), it is clear that while the first term on the right-hand-side (involving invariant J_2) captures deformation rate ($\dot{\mathbf{C}}$) dependence on stress, the second term, via invariant J_5, allows for any interaction effects that may exist between the instantaneous deformation and its rate of change with respect to time ($\mathbf{C}\cdot\dot{\mathbf{C}}$ and $\dot{\mathbf{C}}\cdot\mathbf{C}$).

Based on Eq. (28), the following generalized form of the viscous dissipation potential is proposed

$$W_v = \sqrt{I_1 - 3}\sum_{i=1}^{N} k_{1i} J_2^{c_{1i}} + \sqrt{I_2 - 3}\sum_{j=1}^{M} k_{2j} J_5^{c_{2j}} \tag{30}$$

where k_{1i}, k_{2j}, c_{1j} and c_{2j} represent the $(N+M)$ model parameters, whose values can be obtained by fitting experimental stress-strain data at various strain rates. By combining Eq. (30) with the general hyperelastic strain energy density function in Eq. (17), a generalized expression for the visco-hyperelastic Cauchy stress $\boldsymbol{\sigma}$ (Eq. (15b)) is obtained as

$$\boldsymbol{\sigma} = -p\mathbf{1} + s_1\mathbf{B} + s_{-1}\mathbf{B}^{-1} + h_{\mathrm{D}}\mathbf{B}\cdot\mathbf{D}\cdot\mathbf{B} + h_{\mathrm{D2}}[\mathbf{B}\cdot(\mathbf{B}\cdot\mathbf{D}\cdot\mathbf{B}) + (\mathbf{B}\cdot\mathbf{D}\cdot\mathbf{B})\cdot\mathbf{B}] \tag{31}$$

where the response functions s_1, s_{-1}, h_{D} and h_{D2} depend on both the model constants and the current values of strain and strain rate, and are given as

$$s_1 = 2\frac{\partial W_h}{\partial I_1} \tag{32a}$$

$$s_{-1} = -2\frac{\partial W_h}{\partial I_2} \tag{32b}$$

$$h_{\mathrm{D}} = 8\sqrt{I_1 - 3}\sum_{i=1}^{N} k_{1i} c_{1i} J_2^{c_{1i}-1} \tag{32c}$$

$$h_{\mathrm{D2}} = 4\sqrt{I_2 - 3}\sum_{j=1}^{M} k_{2j} c_{2j} J_5^{c_{2j}-1} \tag{32d}$$

The present work is the first to define rate-dependent response functions h_{D} and h_{D2} for the formulation of the generalized visco-hyperelastic Cauchy stress tensor. For a simple shear deformation (Fig. 2(a)), by using the tensors and invariants from Eq. (21), $J_5 = \dot{\gamma}^2(4\gamma^4 + 9\gamma^2 + 2)$ using Eq. (14), the condition $\mathrm{tr}(\boldsymbol{\sigma}) = 0$ to obtain the indeterminate Lagrange multiplier p, and transforming to the reference configuration, the nominal shear stress is obtained as

$$T_{21}^0 = 2\left(\tfrac{\partial W_h}{\partial I_1} + \tfrac{\partial W_h}{\partial I_2}\right)\gamma + \sum_{i=1}^{N} 2^{c_{1i}+1} k_{1i} c_{1i} \dot{\gamma}^{2c_{1i}-1} \gamma\left(1 + 2\gamma^2\right)^{c_{1i}} + \sum_{j=1}^{M} 2^{c_{2j}+1} k_{2j} c_{2j} \dot{\gamma}^{2c_{2j}-1} \gamma\left(2\gamma^4 + \tfrac{9}{2}\gamma^2 + 1\right)^{c_{2j}} \tag{33}$$

Further, the infinitesimal strain shear modulus is obtained by taking the limit of the derivative with respect to γ at $\gamma \to 0$

$$G_0 = G_{0,h} + \sum_{i=1}^{N} 2^{c_{1i}+1} k_{1i} c_{1i} \dot{\gamma}^{2c_{1i}-1} + \sum_{j=1}^{M} 2^{c_{2j}+1} k_{2j} c_{2j} \dot{\gamma}^{2c_{2j}-1} \tag{34}$$

Using the same approach, this time with the invariants and tensors from Eq. (25), $J_5 = 2\dot{\lambda}^2(2\lambda^4 + \frac{1}{\lambda^5})$ using Eq. (14), and the condition of uniaxial deformation, i.e., $\sigma_{22} = \sigma_{33} = 0$, the nominal uniaxial stress is given by

$$\begin{aligned} T_{11}^0 = {} & 2\tfrac{\partial W_h}{\partial I_1}\left(\lambda - \tfrac{1}{\lambda^2}\right) + 2\tfrac{\partial W_h}{\partial I_2}\left(1 - \tfrac{1}{\lambda^3}\right) + \sum_{i=1}^{N} 2^{c_{1i}+1} k_{1i} c_{1i} \left(\dot{\lambda}\right)^{2c_{1i}-1} \left(2\lambda^2 + \tfrac{1}{\lambda^4}\right)^{c_{1i}} \sqrt{\lambda^2 + \tfrac{2}{\lambda} - 3} + \\ & \sum_{j=1}^{M} 2^{c_{2j}+1} k_{2j} c_{2j} \left(\dot{\lambda}\right)^{2c_{2j}-1} \left(2\lambda^4 + \tfrac{1}{\lambda^5}\right)^{c_{2j}} \sqrt{2\lambda + \tfrac{1}{\lambda^2} - 3} \end{aligned} \tag{35}$$

Further, the infinitesimal strain modulus during uniaxial deformation is obtained by taking the limit of the derivative with respect to λ at $\lambda \to 1$

$$E_0 = E_{0,h} + \sum_{i=1}^{N} 2^{c_{1i}+1} 3^{c_{1i}+\frac{1}{2}} k_{1i} c_{1i} \left|\dot{\lambda}\right|^{2c_{1i}-1} + \sum_{j=1}^{M} 2^{c_{2j}+1} 3^{c_{2j}+\frac{1}{2}} k_{2j} c_{2j} \left|\dot{\lambda}\right|^{2c_{2j}-1} \tag{36}$$

From Eqs. (34) and (36), it is clear that the proposed generalized viscous dissipation potential (Eq. (30)) not only enables modeling of strain rate sensitivity, but also permits flexibility in the relation between elastic moduli (and hence the Poisson's ratio) and strain rate through its model parameters. That is, while k_{1i} and k_{2j} control the rate of increase of elastic moduli with applied strain rate, c_{1i} and c_{2j} are related to the curvature associated with this change. Accordingly, in this study, the parameters k_{1i} and k_{2j} are called the "rate sensitivity control parameters", and c_{1i} and c_{2j} are called the "rate sensitivity indices".

3.2. Particular form for further investigation

An efficient and reliable constitutive model should contain the minimum number of model parameters necessary to capture the essential features of a given experimental phenomenon (Beda, 2014; Yang et al., 2000). Excessive number of model parameters not only render the mathematical form overly complicated and non-physical, but may also lead to non-unique optimal parameter sets, especially in case of nonlinear formulations (Ogden et al., 2004; Puglisi and Saccomandi, 2016). With this motivation, the following reduced form (N, $M=1$, $c_{11}=1$) of Eq. (30) is proposed

$$W_v = k_{11}\sqrt{I_1-3}J_2 + k_{21}\sqrt{I_2-3}J_5^{c_{21}} \tag{37}$$

In Eq. (37), k_{11} is the linear rate sensitivity control parameter, which is associated with a linearly increasing elastic modulus with strain rate (consider $c_{1i}=1$ in Eqs. (34) and (36)), and k_{21} and c_{21} are the nonlinear rate sensitivity control parameter and the strain rate sensitivity index, respectively.

In addition to fewer model parameters, a good judgement of initial guesses (starting point for optimization) during nonlinear least-square fitting with experimental data is crucial in achieving unique model parameters (Beda, 2014; Destrade et al., 2017). Random initial guessing of model parameters can lead to very different optimum solution sets while fitting the same experimental data, which is a serious drawback of many popular nonlinear hyperelastic constitutive models whose parameters lack physical significance (e.g., Ogden model (Ogden, 1972)). The proposed viscous dissipation potential's only nonlinear model constant, c_{21}, holds a physical meaning pertaining to the curvature of the increase of initial moduli with strain rate, and thus can be estimated a priori by plotting experimentally obtained elastic modulus versus strain rate data. This leads to a reasonable estimate for the initial guess as well as a measure to discard unreasonable solutions a posteriori. In this way, the proposed dissipation potential can capture nonlinear strain rate sensitivity effects, and at the same time prevents the numerical instabilities associated with nonlinear models.

The Cauchy stress tensor (Eqs. (31) and (32)) and the nominal stresses under simple shear and uniaxial deformation (Eqs. (33) and ((35)) are obtained for a visco-hyperelastic model with Eq. (37) as the viscous dissipation potential as

$$\begin{aligned}&\boldsymbol{\sigma} = \boldsymbol{\sigma}_h + \boldsymbol{\sigma}_v = -p\mathbf{1} + 2\frac{\partial W_h}{\partial I_1}\mathbf{B} - 2\frac{\partial W_h}{\partial I_2}\mathbf{B}^{-1} + 8\sqrt{I_1-3}k_{11}\mathbf{B}\cdot\mathbf{D}\cdot\mathbf{B} + \\ &4\sqrt{I_2-3}k_{21}c_{21}J_5^{c_{21}-1}[\mathbf{B}\cdot(\mathbf{B}\cdot\mathbf{D}\cdot\mathbf{B}) + (\mathbf{B}\cdot\mathbf{D}\cdot\mathbf{B})\cdot\mathbf{B}]\end{aligned} \tag{38a}$$

$$T_{21}^0 = 2\left(\frac{\partial W_h}{\partial I_1} + \frac{\partial W_h}{\partial I_2}\right)\gamma + 4k_{11}\dot{\gamma}\gamma\left(1+2\gamma^2\right) + 2^{c_{21}+1}k_{21}c_{21}\dot{\gamma}^{2c_{21}-1}\gamma\left(2\gamma^4 + \frac{9}{2}\gamma^2 + 1\right)^{c_{21}} \tag{38b}$$

$$\begin{aligned}&T_{11}^0 = 2\tfrac{\partial W_h}{\partial I_1}\left(\lambda - \tfrac{1}{\lambda^2}\right) + 2\tfrac{\partial W_h}{\partial I_2}\left(1 - \tfrac{1}{\lambda^3}\right) + 4k_{11}\dot{\lambda}\left(2\lambda^2 + \tfrac{1}{\lambda^4}\right)\sqrt{\lambda^2 + \tfrac{2}{\lambda} - 3} + \\ &2^{c_{21}+1}k_{21}c_{21}\left(\dot{\lambda}\right)^{2c_{21}-1}\left(2\lambda^4 + \tfrac{1}{\lambda^5}\right)^{c_{21}}\sqrt{2\lambda + \tfrac{1}{\lambda^2} - 3}\end{aligned} \tag{38c}$$

The above equations will be used in the modeling of experimental stress versus strain response under different primary deformation modes. A detailed description and background of the fitting procedure can be found in the supplementary material. Briefly, the purely hyperelastic model parameters are obtained from the quasi-static experiment data (lowest strain rate) under different deformation modes using linear or nonlinear least squares optimization depending on the selected model type. Once the hyperelastic model parameters are obtained, data from higher strain rate tests are added to the objective function (see supplementary material) and a nonlinear least squares optimization algorithm is used to determine the remaining model constants. In particular, the *Lsqcurvefit* function of MATLAB is used with the trust-region-reflective (TR) method (Coleman and Li, 1996). As stated earlier, the nonlinear parameter obtained from the shear and uniaxial modulus versus strain rate plots (if available) is used as the initial starting point. In addition, the necessary limit of the strain rate sensitivity index ($c_{21} > (1/2)$; see the supplementary material) is used to provide a lower bound for the solution search. The convergence criterion is set such that the algorithm stops when either the Newton step becomes smaller than 10^{-8}, the supremum norm of the objective function gradient becomes less than 10^{-12}, or the number of iterations surpass 3000. To further ensure uniqueness of the obtained model parameters, a multi-start optimization is conducted by defining a uniform distribution grid of 120 points around the initial guesses (c_{21} bounded to ± 2; bounds for control parameters decided on a case-by-case basis). Only the globally minimum solution is selected as the optimal set of model parameters. It is verified that the same unique global solution is obtained even if the grid density is increased (doubled or tripled). The relative errors are calculated for each deformation mode and strain rate as the measure of the goodness of fit

$$\mathrm{err}_i = \frac{\left|f_i(\Lambda_i, \boldsymbol{p}^*) - \boldsymbol{\tau}_i^{0,\mathrm{exp}}\right|}{\max\left\{0.1\max\left(\boldsymbol{\tau}^{0,\mathrm{exp}}\right), \boldsymbol{\tau}_i^{0,\mathrm{exp}}\right\}},\ i = 1, 2, \ldots, m \tag{39}$$

where $\tau_i^{0,exp}$ is the i^{th} data-point of the measured nominal stress at some strain value Λ_i, and $f_i(\Lambda_i, \boldsymbol{p}^*)$ is the i^{th} component of the vector containing symbolic nominal stress equations formulated using a particular visco-hyperelastic model, $\boldsymbol{p}^*$ being the optimized model constants. Note that the term $(0.1\max(\boldsymbol{\tau}^{0,\,exp}))$ is added in the denominator to avoid division by very small stresses in the small strain regime, which otherwise would result in fallaciously large error values.

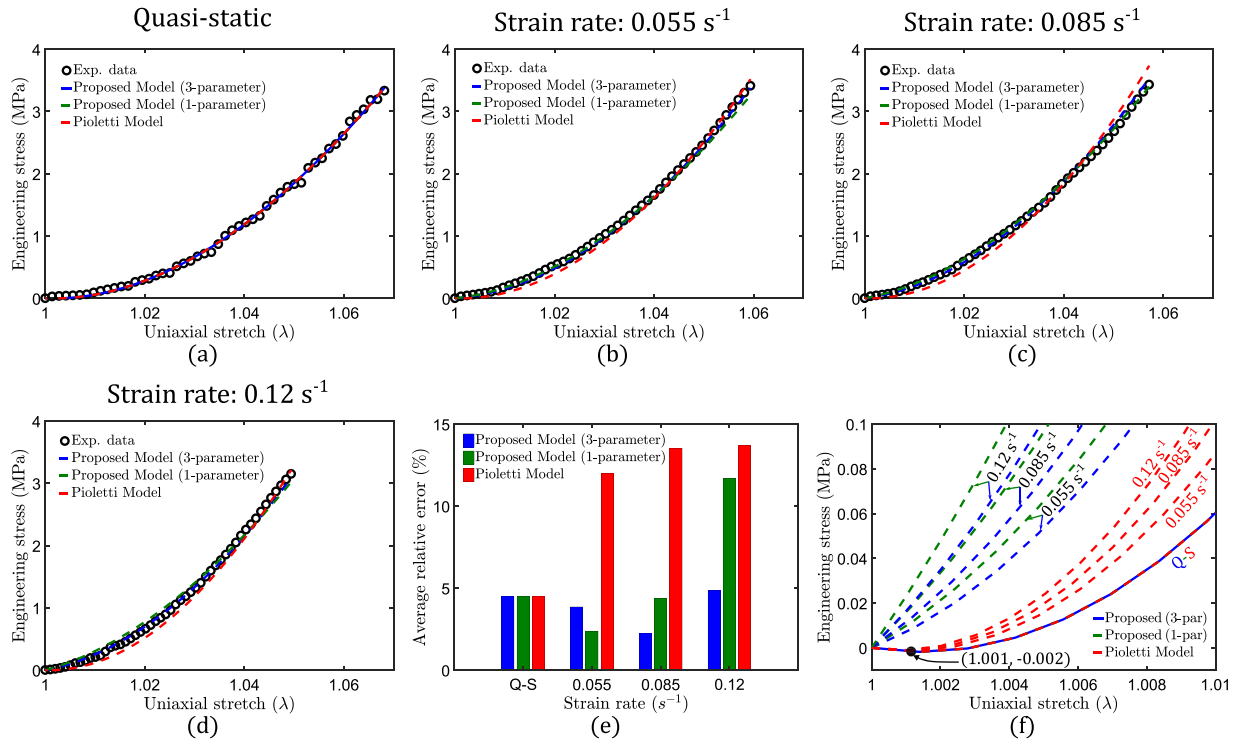

Fig. 3. Experimentally obtained uniaxial tension stress-strain data of patellar tendon and its numerical fitting using the Pioletti and the proposed visco-hyperelastic models (3- and 1-parameter) at various strain rates: (a) quasi-static (0.003 s^{-1}), (b) 0.055 s^{-1}, (c) 0.85 s^{-1}, and (d) 0.12 s^{-1}. (e) Comparison of the average (%) relative errors at different strain rate levels. (f) Model response in the small strain regime (<1%), showing that the Mooney-Rivlin model results in a physically implausible compressive stress for a tensile strain in this region.

4. Model performance comparison with an existing viscous dissipation potential

So far, two advancements over the existing viscous dissipation potentials in the literature are clear: the proposed potential (Eq. (37)) is based on physically motivated parameters and provides the capability to flexibly capture the strain rate sensitivity of stress-strain data in the small strain regime. In this section, the fitting performance of a visco-hyperelastic model formulated using the proposed viscous dissipation potential is compared with that formulated using an existing viscous dissipation potential. Specifically, the rate-dependent tensile response of human patellar tendon as reported by Pioletti et al. (1998) is investigated, which was modeled by these authors using the first external state variable-based viscous dissipation potential (hereinafter referred to as the Pioletti model)

$$W_v = W_v(I_1, J_2) = \frac{\eta'}{4}(I_1 - 3)J_2 \tag{40}$$

where η' is a model parameter. As Eq. (40) consists of only a single model parameter, a reduced one-parameter form of the proposed dissipation potential ($k_{21} = 0$) is also considered for comparison. A two-parameter Mooney-Rivlin model ($W_h = A_{10}(I_1 - 3) + A_{01}(I_2 - 3)$; A_{10} and A_{01} are model constants) is used as the hyperelastic strain energy density function in all cases. The resulting visco-hyperelastic uniaxial nominal stress equations for the proposed models (from Eq. (38c)) are

$$\text{Proposed model (3-parameter)}: \; T_{11}^0 = 2A_{10}\left(\lambda - \tfrac{1}{\lambda^2}\right) + 2A_{01}\left(1 - \tfrac{1}{\lambda^3}\right) + 4k_{11}\dot{\lambda}\left(2\lambda^2 + \tfrac{1}{\lambda^4}\right)\sqrt{\lambda^2 + \tfrac{2}{\lambda} - 3} + 2^{c_{21}+1}k_{21}c_{21}\left(\dot{\lambda}\right)^{2c_{21}-1}\left(2\lambda^4 + \tfrac{1}{\lambda^5}\right)^{c_{21}}\sqrt{2\lambda + \tfrac{1}{\lambda^2} - 3} \tag{41a}$$

$$\text{Proposed model (1-parameter)}: \quad T_{11}^0 = 2A_{10}\left(\lambda - \tfrac{1}{\lambda^2}\right) + 2A_{01}\left(1 - \tfrac{1}{\lambda^3}\right) + 4k_{11}\dot{\lambda}\left(2\lambda^2 + \tfrac{1}{\lambda^4}\right)\sqrt{\lambda^2 + \tfrac{2}{\lambda} - 3} \tag{41b}$$

In case of the Pioletti model (Pioletti et al., 1998), the visco-hyperelastic uniaxial nominal stress equation from Eq. (26) (by substituting $\beta = 1$ and $\eta = (\eta'/4)$) is

$$\text{Pioletti Model}: \quad T_{11}^0 = 2A_{10}\left(\lambda - \tfrac{1}{\lambda^2}\right) + 2A_{01}\left(1 - \tfrac{1}{\lambda^3}\right) + \eta'\dot{\lambda}\left(\lambda^2 + \tfrac{2}{\lambda} - 3\right)\left(2\lambda^2 + \tfrac{1}{\lambda^4}\right) \tag{42}$$

Eqs. (41) and (42) are now used to fit the experimental uniaxial tension data. Fig. 3 compares the fitted curves to the experimental data and Table 1 lists the obtained model parameters and average residual error (from Eq. (39)). Note, all three

Table 1
Model parameters and overall average residual error of fit across the investigated strain rates obtained using the proposed visco-hyperelastic (Eq. (41)) and Pioletti et al. (1998) (Eq. (42)) models.

Proposed visco-hyperelastic model (3-parameter)					
A_{10} (MPa)	A_{01} (MPa)	k_{11} (MPa.s)	k_{21} (MPa.s)	c_{21}	$\overline{\text{err}}$ (%)
144.29	−144.71	−67.18	74.05	1.00	3.85

Proposed visco-hyperelastic model (1-parameter)			
A_{10} (MPa)	A_{01} (MPa)	k_{11} (MPa.s)	$\overline{\text{err}}$ (%)
144.29	−144.71	9.90	5.73

Pioletti et al. (1998)			
A_{10} (MPa)	A_{01} (MPa)	η' (MPa.s)	$\overline{\text{err}}$ (%)
144.29	−144.71	545.2	10.92

models assume material incompressibility, which is a common assumption for most biological tissues and gels because they consist mostly of water (Wex et al., 2015).

The quasi-static stress-strain response of all three models are identical (Fig. 3(a)) because the same hyperelastic model is used. Under dynamic strain rates (Figs. 3(b–d)), both the one and three-parameter forms of the proposed model perform better in capturing the experimental data when compared to the Pioletti model. This is also evident from the average residual errors in Fig. 3(e). As the Pioletti model is rate-insensitive in the small strain regime (does not allow elastic moduli to change), the deviation of its fitted response from the experimental data is prominent in the early part of the dynamic stress-strain plots. This leads to an early peak in the relative error versus stretch plots (see the supplementary material). The proposed viscous dissipation potential captures rate sensitivity of elastic moduli, and thus such error peaks are mitigated. Note, the strain rate sensitivity index c_{21} of the three-parameter form of the proposed viscous dissipation potential is unity (Table 1), which indicates a linearly rate sensitive mechanical response. Interestingly, with the same number of model parameters, the single-parameter form of the proposed viscous dissipation potential reduces the average residual fitting errors to approximately half when compared to the Pioletti model (see Table 1). Therefore, the proposed model offers a considerable improvement in fitting performance over the Pioletti model.

From Table 1, the obtained hyperelastic constants from quasi-static stress-strain data do not follow the necessary condition of thermodynamic stability for the Mooney-Rivlin model in uniaxial deformation ($(A_{10} + A_{10}) > 0$) as suggested by Upadhyay et al., 2019b. This is evident from the region of the tensile stress-strain curve very close to zero strain as shown in Fig. 3(f), where the Mooney-Rivlin model predicts a negative (compressive) stress under a tensile stretch, which is a physically implausible state. While the elastic modulus in the proposed model increases with strain rate, thus ensuring thermodynamic stability of the dynamic response, it remains constant in the case of Pioletti model, which yields a physically implausible infinitesimal strain response in every dynamic strain rate level (see Fig. 3(f)). Consequently, the proposed viscous dissipation potential prevents the choice of quasi-static hyperelastic model from exclusively determining the stability of the modeled stress-strain data, which underscores an important advantage of using it in viscous dissipation-based visco-hyperelastic models.

Note, although the thermodynamic constitutive (T-C) inequality for the polynomial hyperelastic models (Upadhyay et al., 2019b) excludes the Mooney-Rivlin model as a reasonable constitutive equation for capturing the quasi-static tensile response of human patellar tendon, the present work makes no attempt to fit a different hyperelastic model to the stress-strain data. This is because for the purposes of comparing the two viscous dissipation potentials (which define the overstress exclusively), only the accuracy of the selected hyperelastic model is of concern and not the thermodynamic acceptability.

The proposed viscous dissipation potential (Eq. (37)) is also employed to individually fit the rate-dependent stress-strain data in the other two primary deformation modes: compression and shear, as shown in Appendix A. In particular, the very high strain rate compression stress-strain data of ballistic gelatin and the simple shear data of porcine brain tissue are investigated. The former allows the investigation of model applicability in a much wider strain rate range and in a system that exhibits nonlinear strain rate sensitivity. Additional single deformation mode examples of Styrene-ethylene-butylene-styrene (SEBS) gel, ballistic gelatin and polydimethylsiloxane (PDMS) elastomer are provided in the supplementary material (compression stress-strain modeling of SEBS gel is compared against a recently proposed extended hyperelastic model used for this material).

5. Combined multi-deformation mode analysis of human brain gray matter

Brain is a complex multiphasic structure composed of white and gray matter, blood vessels, membranes, voids, and fissures, all filled with or surrounded by cerebrospinal fluid. The mechanical response varies between these tissue types, brain-region where specimens are extracted from, and also the age and gender of the test subjects (van Dommelen et al., 2009). The average mechanical response of brain tissue has been modeled extensively using globally isotropic constitutive equations (e.g., refer (Mihai et al., 2017) for a review of isotropic hyperelastic models used for modeling brain tissue). It is now well established that while gray matter is nearly isotropic, white matter is anisotropic (Budday et al., 2015; Prange et al.,

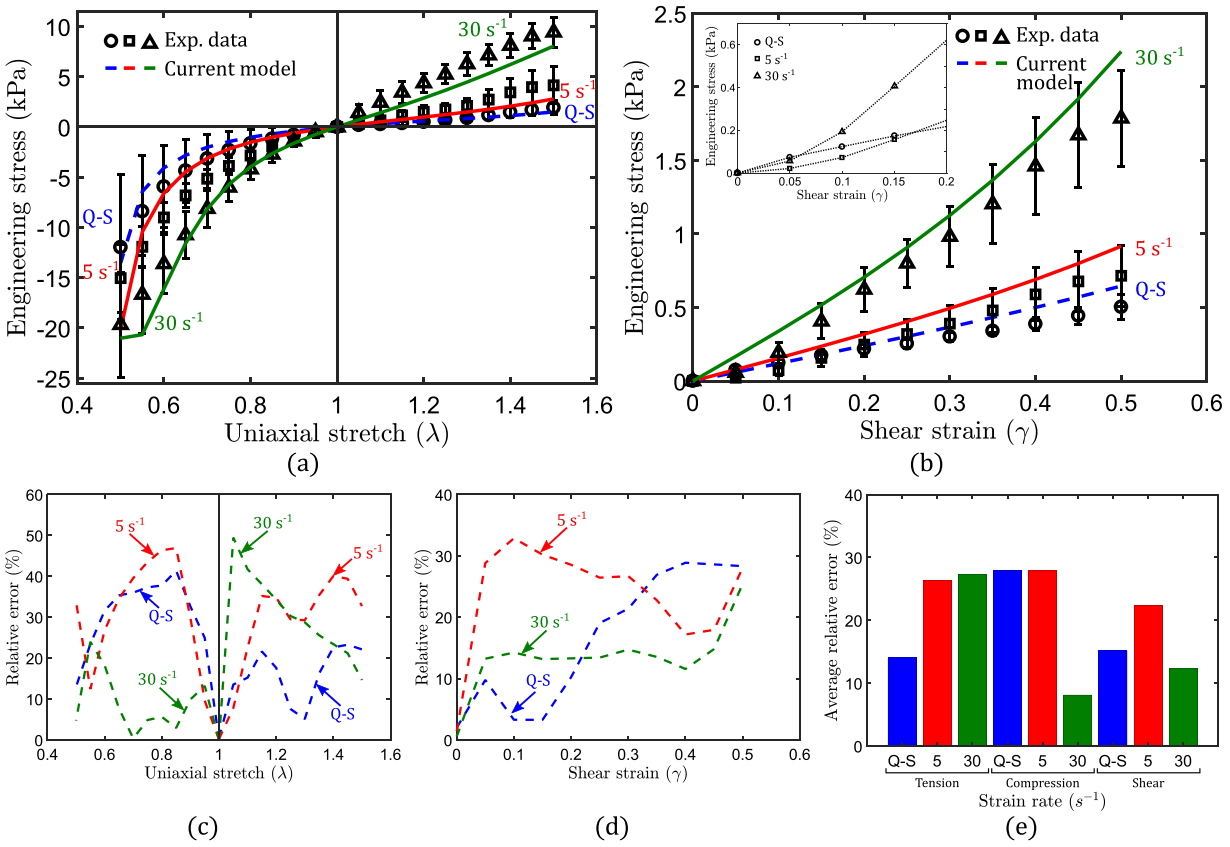

Fig. 4. Experimentally obtained stress-strain plots of human brain tissue gray matter in (a) uniaxial and (b) simple shear deformation, and the numerically fitted response obtained using the proposed visco-hyperelastic model. Inset of (b) shows the zoomed-in shear response for < 20% shear strain. Plots of relative errors (%) versus (c) uniaxial stretch and (d) nominal shear strain. (e) Average (%) relative errors at different strain rate levels and deformation modes.

2000; Prange and Margulies, 2002). As the proposed viscous dissipation potential assumes material to be isotropic, in this section, the strain rate dependent multimodal deformation response of human gray matter under compression, tension and shear as reported by Jin et al. (2013) is investigated. The simultaneous consideration of multiple deformation modes extends the single deformation-mode analysis conducted in the previous subsection, and will highlight the versatility of the proposed model.

Figs. 4(a) and (b) show stress-strain responses under uniaxial (compression and tension) and shear deformation at three strain rate levels with reported error bars, respectively. The inset in Fig. 4(b) shows the experimentally reported shear stress-strain data for shear strain $\gamma < 0.2$. Notice the order of shear stress values for the three investigated strain rates in this region (data points corresponding to $\gamma = 0.05$, 0.10 and 0.15). Based on the entire uniaxial response and the shear response for $\gamma \geq 0.2$, the stress at a particular strain increases with strain rate (a stiffening behavior). This, however, is not noticed in this small strain region ($\gamma < 0.2$), where, for example, the reported quasi-static stress for $\gamma = 0.05$ is greater than both dynamic stresses (5 s^{-1} and 30 s^{-1}). It seems that this "softening" behavior is an experimental error, the probable reasons being poor accuracy of load-cell during low load, or issues regarding determination of reference position in soft materials testing (Destrade et al., 2017; Vogel et al., 2017). Therefore, the three data points in this region corresponding to $\gamma = 0.05$, 0.10 and 0.15 are disregarded in numerical analysis; in place of these values, the interpolated values based on the rest of the data are used.

To model the quasi-static stress-strain data, the semi-empirical Gent-Gent model (Pucci and Saccomandi, 2002) is used. The reason behind choosing this model is its physical interpretation in regard to the molecular (non-Gaussian statistical) theory (Puglisi and Saccomandi, 2016) and its ability to fit both single and combined deformation modes with reasonable accuracy and only three model parameters (Ogden et al., 2004). Mathematically, the Gent-Gent strain energy density function is

$$W_h = -\frac{\mu J_m}{2}\ln\left(1-\frac{I_1-3}{J_m}\right)+\frac{3C_2}{2}\ln\left(\frac{I_2}{3}\right) \tag{43}$$

where μ, J_m and C_2 are model parameters. Note that J_m represents the limiting value of $I_1 - 3$, when molecular chains in a polymer network are in their fully stretched state. By combining the quasi-static strain energy density in Eq. (43) with the

Table 2
Model parameters and overall average residual error of fit when combined tension-compression-shear response of human brain gray matter (Jin et al., 2013) is modeled using the proposed visco-hyperelastic model (Eq. (44)).

μ (kPa)	J_m	C_2 (kPa)	k_{11} (Pa.s)	k_{21} (Pa.s)	c_{21}	$\overline{\text{err}}$ (%)
0.73	1.60	0.46	18.03	−2.29E-6	2.28	20.14

proposed viscous dissipation potential (Eq. (37)), a six-parameter visco-hyperelastic constitutive model is formulated; the uniaxial and simple shear nominal stresses are given by (Eqs. (38b) and (38c))

$$T_{11}^0 = \frac{\mu J_m}{J_m - \left(\lambda^2 + \frac{2}{\lambda} - 3\right)}\left(\lambda - \frac{1}{\lambda^2}\right) + \frac{3C_2\left(1 - \frac{1}{\lambda^3}\right)}{\left(2\lambda + \frac{1}{\lambda^2}\right)} + 4k_{11}\dot{\lambda}\left(2\lambda^2 + \frac{1}{\lambda^4}\right)\sqrt{\lambda^2 + \frac{2}{\lambda} - 3} + 2^{c_{21}+1}k_{21}c_{21}\left(\dot{\lambda}\right)^{2c_{21}-1}\left(2\lambda^4 + \frac{1}{\lambda^5}\right)^{c_{21}}\sqrt{2\lambda + \frac{1}{\lambda^2} - 3} \tag{44a}$$

$$T_{21}^0 = \frac{\mu J_m \gamma}{J_m - \gamma^2} + \frac{3C_2\gamma}{\gamma^2 + 3} + 4k_{11}\dot{\gamma}\gamma\left(1 + 2\gamma^2\right) + 2^{c_{21}+1}k_{21}c_{21}\dot{\gamma}^{2c_{21}-1}\gamma\left(2\gamma^4 + \frac{9}{2}\gamma^2 + 1\right)^{c_2} \tag{44b}$$

Figs. 4(a) and (b) show the numerically fitted stress-strain curves using Eqs. (44a) and (44b) in uniaxial and shear states, respectively; corresponding relative errors of fit are shown in Figs. 4(c) and (d). Table 2 lists the obtained model parameters and the overall average residual error of fit.

From Table 2, it can be inferred that the overall mechanical response of human brain gray matter is nearly linearly rate sensitive with a very small nonlinear rate sensitivity control parameter k_{21}; disregarding this parameter completely (using $k_{21} = 0$) increases fitting error to 21.59% (visible fitting change only in the large strain region of compression stress-strain plot at 30 s^{-1} strain rate). Fig. 4(e) compares the average relative errors for different applied strain rates. The Gent-Gent model in quasi-static tension, compression and shear results in average fitting errors of 14.01%, 27.89% and 15.13%, respectively; these average errors become 26.83%, 17.99% and 17.32% in the dynamic regime when the proposed viscous dissipation potential is added to formulate the visco-hyperelastic model (Eqs. (44a) and (44b)). Clearly, by adding only three viscous parameters to the quasi-static hyperelastic model, the proposed visco-hyperelastic model captures all the major features of the dynamic stress-strain data and results in a similar level of accuracy as the quasi-static fit. The present study is the first to model simultaneously all three primary deformation modes of human brain gray matter in both quasi-static and dynamic strain rates.

For an additional example of porcine brain tissue in combined compression and tension, see the supplementary material.

6. Robustness of the proposed viscous dissipation potential

In this section, the compression-tension-shear stress-strain data of human brain gray matter (Jin et al., 2013) is further analyzed using visco-hyperelastic models based on the proposed viscous dissipation potential to investigate their robustness with respect to two factors: (i) choice of the hyperelastic strain energy density function for quasi-static data fitting, and (ii) availability of data from different deformation modes.

One desirable feature of a visco-hyperelastic model is its robustness with respect to the choice of hyperelastic strain energy density function. To evaluate this, the Gent-Gent model (Eq. (43)) is replaced with three common polynomial-based hyperelastic models and one logarithmic Gent model (Gent, 1996) to formulate different visco-hyperelastic models with a common viscous dissipation potential (Eq. (37)). The strain energy density forms of these hyperelastic models are given as

$$\text{2-parameter Mooney} - \text{Rivlin}: \; W_h = A_{10}(I_1 - 3) + A_{01}(I_2 - 3) \tag{45a}$$

$$\text{3-parameter Mooney} - \text{Rivlin}: \; W_h = A_{10}(I_1 - 3) + A_{01}(I_2 - 3) + A_{11}(I_1 - 3)(I_2 - 3) \tag{45b}$$

$$\text{5-parameter Mooney} - \text{Rivlin}: \; W_h = A_{10}(I_1 - 3) + A_{01}(I_2 - 3) + A_{11}(I_1 - 3)(I_2 - 3) + A_{20}(I_1 - 3)^2 + A_{02}(I_2 - 3)^2 \tag{45c}$$

$$\text{Gent}: \; W_h = -\frac{\mu J_m}{2}\ln\left(1 - \frac{I_1 - 3}{J_m}\right) \tag{45d}$$

The obtained model parameters from the visco-hyperelastic modeling of the combined tension-compression-shear data of human brain gray matter (Jin et al., 2013) are listed in Table 3.

From Table 3, it is clear that the individual model parameters of the polynomial-based hyperelastic models do not show any correlation even when fitting the same quasi-static data. On the other hand, the common model parameters of the quasi-static Gent and Gent-Gent models (μ and J_m) have similar values. Likewise, the model parameters of the proposed viscous dissipation potential also retain similar values (range of values are k_{11} ~ 17–19 Pa.s; k_{21} ~ 0 Pa.s; c_{21} ~ 2.01–2.28).

Table 3
Model parameters obtained when combined tension-compression-shear response of human brain gray matter (Jin et al., 2013) is modeled using the visco-hyperelastic model based on the proposed viscous dissipation potential but with different choices of hyperelastic strain energy density function.

Hyperelastic model choice	Model parameters			
	Quasi-static		Dynamic	
	Name	Value (kPa)	Name	Value (Pa.s)
2-parameter Mooney-Rivlin	A_{10}	−0.06	k_{11}	17.61
	A_{01}	0.71	k_{21}	−3.56E-6
			c_{21} (dimensionless)	2.23
3-parameter Mooney-Rivlin	A_{10}	0.21	k_{11}	18.22
	A_{01}	0.35	k_{21}	−4.99E-5
	A_{11}	0.24	c_{21} (dimensionless)	2.01
5-parameter Mooney-Rivlin	A_{10}	−0.97	k_{11}	17.41
	A_{01}	1.58	k_{21}	−6.97E-6
	A_{11}	−7.26	c_{21} (dimensionless)	2.18
	A_{20}	4.68		
	A_{02}	2.59		
Gent	μ	1.12	k_{11}	18.47
	J_m	1.75	k_{21}	−9.74E-6
			c_{21} (dimensionless)	2.15
Gent-Gent	μ	0.76	k_{11}	18.03
	J_m	1.60	k_{21}	−2.29E-6
	C_2	0.46	c_{21} (dimensionless)	2.28

Table 4
Model parameters of the proposed visco-hyperelastic model obtained by fitting different sets of single and multiple deformations, and the associated average fitting error when data of combined tension-compression-shear is predicted (individual mode fitting errors are listed in square brackets; C, T, and S represent compression, tension and shear, respectively).

Deformation mode(s) considered	μ (kPa)	J_m	C_2 (kPa)	k_{11} (Pa.s)	k_{21} (Pa.s)	c_{21}	$\overline{\text{err}}$ (%)
Compression only	6.58	6.87	−3.72	11.64	−2.79E-5	2.01	66.20 [C 9.18, T 80.37, S 109.05]
Compression + Tension	−0.18	3839.63	1.88	23.21	−2.10E-2	1.50	28.36 [C 23.70, T 14.71, S 46.67]
Compression + Tension + Shear	0.76	1.60	0.46	18.03	−2.29E-6	2.28	20.14 [C 21.28, T 22.56, S 16.59]

This highlights the robustness of the proposed viscous dissipation potential in capturing the strain rate dependent stress-strain response, which is not contingent on the choice of a particular quasi-static hyperelastic strain energy density equation.

Another desirable feature of a constitutive model is its robustness with respect to other deformation modes (Destrade et al., 2017). For example, it has been shown that the Ogden model parameters obtained by fitting tension stress-strain data can be completely different from those obtained by fitting equi-biaxial data, leading to a very poor prediction in the latter deformation (Ogden et al., 2004). At the same time, if both deformation modes were considered together, then a good agreement between model and experimental data was observed. Yielding very different set of model parameters from different experiments is an undesirable behavior, especially in modeling dynamic response of soft materials where certain deformation modes (e.g., unconfined compression) are more commonly tested than the others (e.g., simple shear). As dynamic uniaxial compression stress-strain data is more commonly reported for many soft materials than tension data (Leclerc et al., 2012; Nie et al., 2009), which in turn is more common than simple shear data (Luo et al., 2019; Upadhyay et al., 2019a), the effect of considering only the more commonly available deformation modes on the extracted model constants needs to be examined. Two cases are investigated, (i) when only compression stress-strain data is used, and (ii) when combined compression-tension stress-strain data is used to obtain the model constants of Eq. (44). The model parameters obtained in these cases are used to predict stress-strain data of all primary deformation modes (including those not considered in fitting).

Table 4 lists the obtained model parameters by using fewer deformation modes, along with those obtained by using all three primary deformation modes (Table 3). In addition, the overall average residual errors of fitting/predicting the three experimental data as well as average residual error for individual deformations (in square brackets) are listed. It is seen that compared to the model parameters of the quasi-static Gent-Gent model (μ, J_m and C_2), which do not show any trend when successive deformation modes are added, the parameters of the proposed model (k_{11}, k_{21} and c_{21}) show lesser change in terms of both magnitude and sign. This exercise highlights the stability and robustness of the proposed model with respect to the availability of deformation data types. A similar robustness was observed when the stress-strain data of porcine brain tissue was modeled using the proposed potential (see the supplementary material). In every case, the fitting accuracy is reduced for the deformation mode that is not considered in the original fitting procedure.

It is important to note that not all materials exhibit similar strain rate sensitivities in every primary deformation mode. For example, based on the uniaxial stress-strain data of annulus fibrosus, Vogel et al. (2017) reported that while the maximum tensile stress doubled when the applied strain rate was increased from ~10^{-4} to 10^{-1} s^{-1}, the maximum compressive stress increased by 15 times during the same strain rate increase. When the proposed viscous dissipation potential is used to individually model these tension and compression responses with the Gent-Gent model for quasi-static fitting, the obtained model constants are $\{k_{11} = 0.00$ MPa.s, $c_{21} = 0.62$, and $k_{21} = 0.14$ MPa.s$\}$ and $\{k_{11} = 0.00$ MPa.s, $c_{21} = 0.67$, and $k_{21} = 0.83$ MPa.s$\}$, respectively. On the other hand, when combined tension-compression data is modeled, model constants are $\{k_{11} = 0.10$ MPa.s, $c_{21} = 0.63$, and $k_{21} = 0.31$ MPa.s$\}$. Clearly, the model parameters vary from one deformation mode to the other in order to accommodate the asymmetric nature of strain rate sensitivities; in this case, the nonlinear rate sensitivity control parameter k_{21} is ~6 times larger in compression as compared to tension. This eventually causes a relatively poor combined fitting accuracy, and a higher-order form of the proposed generalized viscous dissipation potential (Eq. (30)) may be required to achieve a better fitting accuracy. On the other hand, for materials in which strain rate sensitivity of individual deformations is not significantly different, the proposed model offers an elegant three-parameter form that captures all major features of the combined stress-strain data with good accuracy.

7. Summary and conclusion

The present study focuses on modeling the visco-hyperelastic short-time memory response of soft materials using the external state variable driven viscous dissipation-based approach, which describes quasi-static equilibrium and dynamic non-equilibrium effects using a hyperelastic strain energy density and a viscous dissipation potential, respectively. As an important contribution of this work, it is demonstrated that all existing viscous dissipation potentials available in the literature lack the ability to capture a generalized strain rate dependence of elastic moduli and Poisson's ratio, which directly conflicts with the abundant experimental evidence of strain rate sensitivity in soft materials. In addition, the parameters of the available models are purely phenomenological. Based on this motivation, a novel viscous dissipation potential form is proposed, which not only allows strain rate dependence of elastic moduli and Poisson's ratio, but is also posed with physically motivated model parameters.

The proposed generalized viscous dissipation potential uses the objective Cauchy-Green deformation tensor and its time rate of change as external state variables via four invariants (I_1, I_2, J_2, and J_5). By combining this form with a general invariant-based hyperelastic strain energy density function, a generalized visco-hyperelastic model is formulated. It is demonstrated that the resulting formulation allows flexible modeling of both linear and nonlinear strain rate effects on elastic moduli via its "rate sensitivity control parameters" and "rate sensitivity indices".

In order to demonstrate the salient features of the proposed model, a reduced three-parameter form of the generalized viscous dissipation potential is formulated, which consists of a linear rate sensitivity control parameter k_{11}, a nonlinear rate sensitivity control parameter k_{21}, and a nonlinear rate sensitivity index c_{21}. While the former two control parameters dictate the rate at which moduli change with strain rate, the latter index defines the curvature associated with this change; thus, the model parameters are based on a physical phenomenon. As the reduced dissipation potential form consists of only a single nonlinear model parameter whose initial guess during numerical optimization can be estimated a priori, it offers mathematical simplicity and promotes uniqueness of optimal model parameters. A multi-step optimization procedure is designed to fit experimental stress-strain data whose search region is restricted via thermodynamics-based inequalities (see supplementary material). A multi-start scheme is used to further validate uniqueness of model parameters and to eliminate local minima. Thus, the proposed formulation captures nonlinear behavior while at the same time preventing numerical instabilities characteristic of many nonlinear constitutive equations (e.g., the Ogden model).

To investigate the advancement in fitting accuracy offered by the proposed dissipation potential compared to existing forms, visco-hyperelastic models based on the Mooney-Rivlin hyperelastic strain energy density are formulated using the proposed viscous dissipation model and an existing Pioletti model to fit uniaxial tension stress-strain data of human patellar tendon. It is demonstrated that the ability of the proposed form to allow strain rate sensitivity in the infinitesimal strain regime not only significantly improves the overall fitting accuracy, but also prevents the thermodynamic stability of the model response from being dictated completely by the choice of the hyperelastic strain energy density function. While the hyperelastic two-parameter Mooney-Rivlin model caused both quasi-static and dynamic model responses to be physically implausible in the early part of the stress-strain curve, the proposed viscous dissipation potential via its strain rate sensitive model parameters prevented thermodynamic instability in the dynamic regime. Thus, an appreciable improvement over existing viscous dissipation-based models is obtained.

In addition, the combined compression-tension-shear response of human brain gray matter is modeled using a visco-hyperelastic model composed of the quasi-static Gent-Gent strain energy density and the proposed viscous dissipation potential. It is seen that with only three additional model parameters, the proposed dissipation potential reasonably captures all the qualitative features of the dynamic response (viscous overstress) and results in a similar level of accuracy as the quasi-static fit. Note, however, that the fitting accuracy is decreased in combined deformation mode fitting as compared to single deformations. Additional single and combined multiple deformation mode applications of different materials are provided in the Appendix A and the supplementary material, which highlights the wider applicability of the proposed form as compared to the existing models. In particular, the ballistic gelatin example demonstrates model applicability in a much wider strain rate range, and the SEBS gel stress-strain modeling comparison with an extended hyperelastic model shows that

the proposed form, in addition to being consistent with both material frame-indifference and continuum thermodynamics principles, provides similar level of accuracy with fewer model parameters.

Further, by replacing the quasi-static portion of the visco-hyperelastic model with different polynomial and logarithmic strain energy density functions, it is shown that the visco-hyperelastic models based on the proposed potential are robust with respect to the choice of the hyperelastic strain energy density equation. Note, however, that the accuracy of the visco-hyperelastic model depends, in part, on the quasi-static strain energy density, and a better hyperelastic model (for a particular case) can reduce overall residual errors in both quasi-static and dynamic regimes. A similar robust response is observed when only compression, compression-tension, and combined compression-tension-shear stress-strain data is fitted using the proposed model; although the fitting accuracy in a particular deformation mode improves when its stress-strain data is considered, the model constants do not show significant changes. Interestingly, the rate sensitivity indices (c_{21}) of all the investigated materials (including those in the supplementary material) exist in a narrow range (0.5–2.3), suggesting stability of this parameter across different materials and its importance in modeling strain rate effects. It is also observed that the viscous overstress is most sensitive to changes in this parameter (see supplementary material).

Recall that the proposed viscous dissipation potential assumes incompressibility and isotropy in the material. While most hydrogels, tissues, and elastomers are nearly incompressible, many soft tissues are anisotropic. In addition, a relatively poor accuracy is obtained when the material exhibits highly asymmetric strain rate sensitivities in different deformation modes. Lack of dynamic stress-strain data over a wide strain rate range in several deformations (e.g., high strain rate stress-strain data in tension and shear) is also an existing challenge. In future work, improvements pertaining to anisotropic modeling and description of asymmetric strain rate sensitivities will be pursued.

Declaration of Competing Interest

The authors declare that they have no known competing financial interests or personal relationships that could have appeared to influence the work reported in this paper.

Acknowledgements

This work was supported by the National Science Foundation under grant nos. CMMI–1634188 and CMMI–1762791 to the University of Florida, Gainesville, USA.

Supplementary materials

Supplementary material associated with this article can be found, in the online version, at doi:10.1016/j.jmps.2019.103777.

Appendix A. Additional single deformation mode examples

A.1. Ballistic gelatin: Uniaxial compression

A popular surrogate material in terminal ballistics, ballistic gelatin is also used in the study of tissue damage during crash/stab wounds and traumatic brain injury (TBI), and as a brain tissue engineering scaffold for tissue regeneration and growth (Sotudeh Chafi et al., 2007; Subhash et al., 2012; Tian et al., 2005; Zhang et al., 2005). Naarayan and Subhash (2017) reported high strain rate compression stress-strain data of 10% w/w ballistic gelatin using polymer split-Hopkinson pressure bar (PSHPB) experiment. Fig. A.1(a) shows the engineering stress-strain plot for five average true strain rate levels. Eq. (41a) is used to numerically fit the data, which is a five-parameter visco-hyperelastic model based on the quasi-static two-parameter Mooney-Rivlin strain energy density; the fitted curves are also shown in Fig. A.1(a). Note that the relation $\dot{\lambda} = \lambda \dot{\varepsilon}_t$ is used to transform the reported true strain rate ($\dot{\varepsilon}_t$) by Naarayan and Subhash (2017) to the engineering strain rate ($\dot{\lambda}$) required in Eq. (41a). The obtained model constants and average error of fit are given in Table A.1.

Fig. A.1(b) shows the percentage relative errors of fit resulting from the proposed model; barring very small strains, a good agreement between the model and the experimental data is observed. The obtained model constants reveal a nonlinear strain rate sensitivity. The average relative error in every strain rate is less than 25% (Fig. A.1(c)); in all but the 2500 s^{-1} strain rate case, the proposed viscous dissipation potential has resulted in an improved fit when compared to the quasi-static fitting by the Mooney-Rivlin model. When compared to the tensile stress-strain data of patellar tendon (Fig. 3), the

Table A.1
Model parameters and overall average residual error of fit when ballistic gelatin compression response (Naarayan and Subhash, 2017) is modeled using the proposed visco-hyperelastic model (Eq. (41a)).

A_{10} (kPa)	A_{01} (kPa)	k_{11} (kPa.s)	k_{21} (kPa.s)	c_{21}	$\overline{\text{err}}$ (%)
46.22	25.47	0.04	−1.16	0.78	16.56

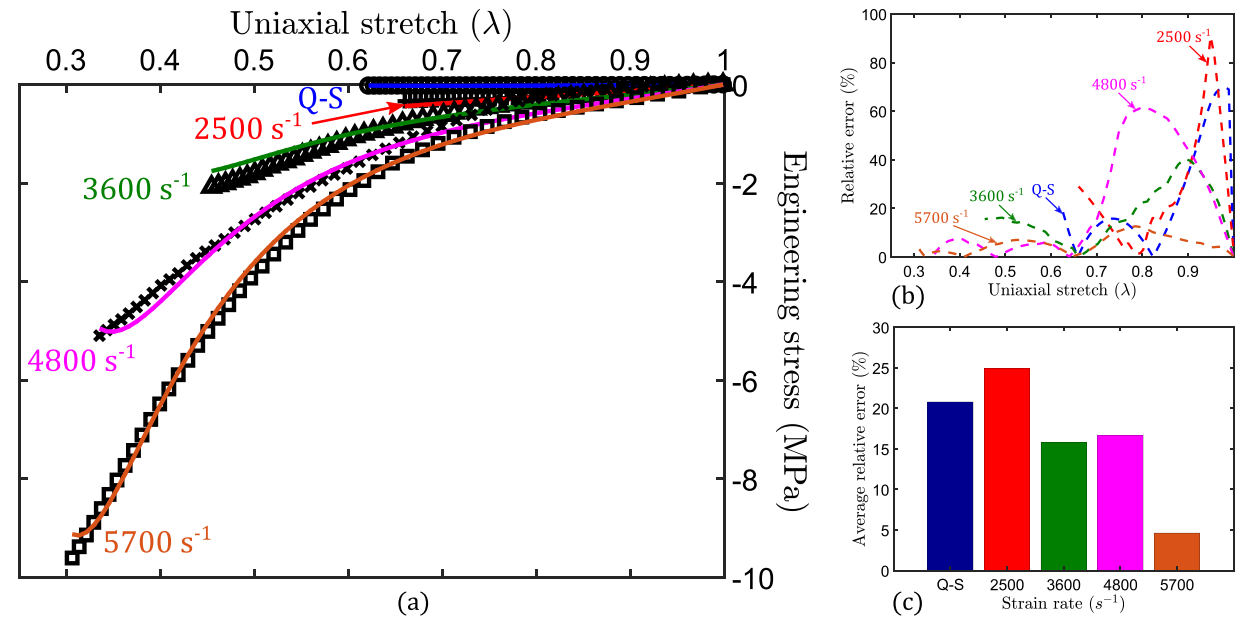

Fig. A.1. (a) Experimentally obtained uniaxial compression stress-strain data of ballistic gelatin (Naarayan and Subhash, 2017) and its numerical fitting using the proposed visco-hyperelastic model. (b) Percentage relative error as a function of uniaxial stretch at various strain rates. (c) Average (%) relative errors at different strain rate (true) levels.

mechanical response of ballistic gelatin in Fig. A.1(a) exhibits larger strains, an increased nonlinearity, and a highly rate sensitive response. The proposed model captures all features of this deformation with good accuracy (average percentage residual, 16.56%), which underlines its utility in large strain visco-hyperelasticity. Interestingly, the error decreases with increasing strain rate, and falls below 5% at the highest strain rate, as shown in Fig. A.1(c).

A.2. Human brain tissue: Simple shear

Donnelly and Medige (1997) studied the average single pulse shear response of human brain tissue under small to moderate strain rates using a single lap shear test. Thirty tests for each of the quasi-static and three dynamic strain rates (30, 60 and 90 s^{-1}) were conducted; the average stress-strain data is shown in Fig. A.2(a). Note, the original stress-strain calculations by Donnelly and Medige (1997) incorrectly computed true shear stress as $\sigma_{12} = T^0_{21}\sqrt{1+\gamma^2}$ citing a "reduced area of the sample" (this error is also noted by Rashid et al. (2013)). The sample area in reality does not change in simple shear, and $\sigma_{12} = T^0_{21}$ holds; this correction has been applied in the stress-strain plots of Fig. A.2(a). It is seen that the quasi-static shear response is highly linear (similar behavior was reported for porcine brain by Rashid et al. (2013)), suggesting suitability of a single-parameter neoHookean model (Rivlin, 1948b; Treloar, 1944) to capture rate-independent response. The proposed viscous dissipation potential function (Eq. (37)) is considered to model the rate-sensitive response; the resulting visco-hyperelastic shear stress is

$$T^0_{21} = 2A_{10}\gamma + 4k_{11}\dot{\gamma}\gamma\left(1+2\gamma^2\right) + 2^{c_{21}+1}k_{21}c_{21}\dot{\gamma}^{2c_{21}-1}\gamma\left(2\gamma^4+\frac{9}{2}\gamma^2+1\right)^{c_{21}} \tag{46}$$

where A_{10} is the model parameter of the neoHookean model ($W_h = A_{10}(I_1-3)$). Note, several studies (Etoh et al., 1994; McElhaney et al., 1973) have reported bulk moduli of brain tissue that are ~10^5 times larger than its shear modulus; thus, the assumption of incompressibility in the present study is well justified. The fitted stress-strain curves using Eq. (46) are shown in Fig. A.2(a); the model constants and average residual error are given in Table A.2.

Table A.2
Model parameters and overall average residual error of fit when human brain tissue shear response (Donnelly and Medige, 1997) is modeled using the proposed visco-hyperelastic model (Eq. (46)).

A_{10} (kPa)	k_{11} (Pa.s)	k_{21} (Pa.s)	c_{21}	$\overline{\text{err}}$ (%)
0.47	12.37	−0.21	1.23	7.18

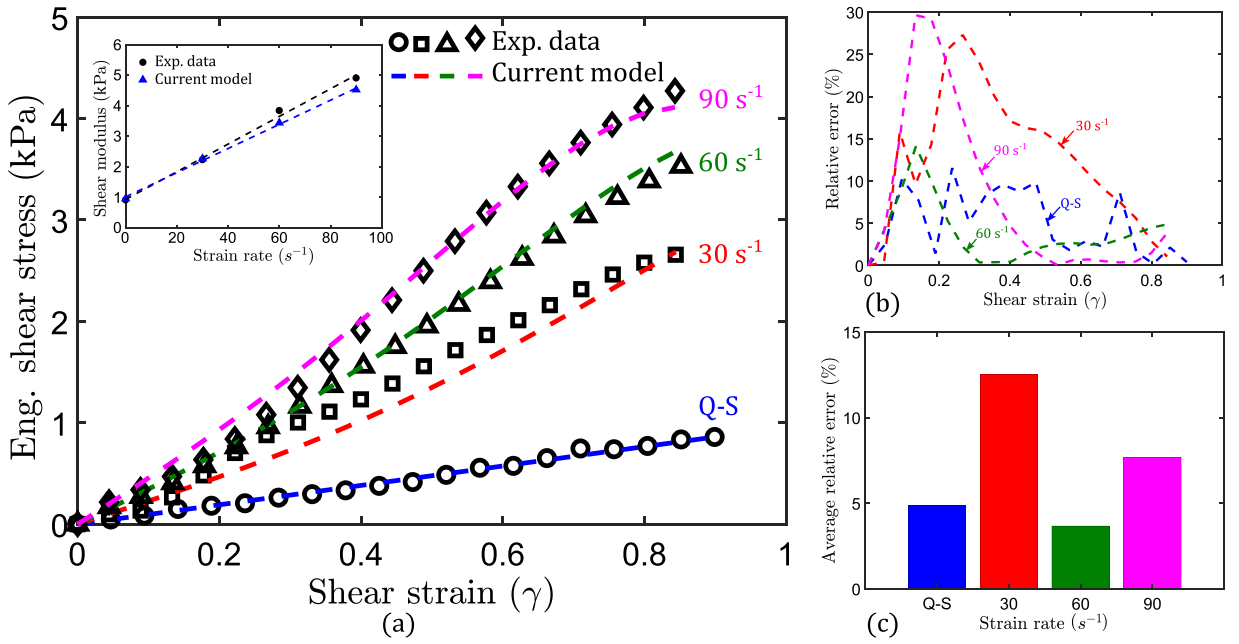

Fig. A.2. (a) Experimentally obtained simple shear stress-strain plots of human brain, and the numerically fitted response obtained using the proposed visco-hyperelastic model; in the inset, the initial shear modulus versus strain rate from the experiments and the proposed model. (b) Relative errors (%) versus shear strain, and (c) average (%) relative errors at the four investigated strain rates.

From the rate sensitivity control parameters and index in Table A.2, it can be inferred that the shear response is nearly linearly strain rate sensitive, with k_{21} two orders of magnitude smaller than k_{11}. This is also apparent from the shear modulus versus strain rate plot shown in the inset of Fig. A.2(a). Both experiments and model show a linear increase in shear modulus with strain rate, further corroborating the ability of the proposed model to accurately capture strain rate sensitivity of elastic moduli. Further, a very good agreement with the experimental stress-strain data is observed (Fig. A.2(b)), which is also evident from the low average residual fitting error (Fig. A.2(c)). Thus, the proposed model, with only four model constants, accurately captures the shear stress-strain response of human brain in the investigated strain rate range.

References

Amin, A.F.M.S., Lion, A., Sekita, S., Okui, Y., 2006. Nonlinear dependence of viscosity in modeling the rate-dependent response of natural and high damping rubbers in compression and shear: experimental identification and numerical verification. Int. J. Plast. 22, 1610–1657. doi:10.1016/j.ijplas.2005.09.005.

Arbogast, K.B., Margulies, S.S., 1998. Material characterization of the brainstem from oscillatory shear tests. J. Biomech. 31, 801–807. doi:10.1016/S0021-9290(98)00068-2.

Arruda, E.M., Boyce, M.C., 1993. A three-dimensional constitutive model for the large stretch behavior of rubber elastic materials. J. Mech. Phys. Solids 41, 389–412. doi:10.1016/0022-5096(93)90013-6.

Avril, S., 2017. Hyperelasticity of soft tissues and related inverse problems. In: Avril, S., Evans, S. (Eds.), Material Parameter Identification and Inverse Problems in Soft Tissue Biomechanics, CISM International Centre for Mechanical Sciences. Springer International Publishing, Cham, pp. 37–66. doi:10.1007/978-3-319-45071-1_2.

Beda, T., 2014. An approach for hyperelastic model-building and parameters estimation a review of constitutive models. Eur. Polym. J. 50, 97–108. doi:10.1016/j.eurpolymj.2013.10.006.

Bergström, J.S., Boyce, M.C., 2000. Large strain time-dependent behavior of filled elastomers. Mech. Mater. 32, 627–644. doi:10.1016/S0167-6636(00)00028-4.

Bergström, J.S., Boyce, M.C., 1998. Constitutive modeling of the large strain time-dependent behavior of elastomers. J. Mech. Phys. Solids 46, 931–954. doi:10.1016/S0022-5096(97)00075-6.

Boehler, J.P. (Ed.), 1987. Applications of tensor functions in solid mechanics, 1st ed.. SpringerVienna, Vienna. 10.1007/978-3-7091-2810-7

Bracq, A., Haugou, G., Bourel, B., Maréchal, C., Lauro, F., Roth, S., Mauzac, O., 2018. On the modeling of a visco-hyperelastic polymer gel under blunt ballistic impacts. Int. J. Impact Eng. 118, 78–90. doi:10.1016/j.ijimpeng.2018.04.001.

Budday, S., Nay, R., de Rooij, R., Steinmann, P., Wyrobek, T., Ovaert, T.C., Kuhl, E., 2015. Mechanical properties of gray and white matter brain tissue by indentation. J. Mech. Behav. Biomed. Mater. 46, 318–330. doi:10.1016/j.jmbbm.2015.02.024.

Coleman, T.F., Li, Y., 1996. An interior trust region approach for nonlinear minimization subject to bounds. SIAM J. Optim. 6, 418–445. doi:10.1137/0806023.

Destrade, M., Saccomandi, G., Sgura, I., 2017. Methodical fitting for mathematical models of rubber-like materials. Proc. R. Soc. A Math. Phys. Eng. Sci. 473, 20160811. doi:10.1098/rspa.2016.0811.

Donnelly, B.R., Medige, J., 1997. Shear properties of human brain tissue. J. Biomech. Eng. 119, 423–432.

Doorly, M.C., Gilchrist, M.D., 2006. The use of accident reconstruction for the analysis of traumatic brain injury due to head impacts arising from falls. Comput. Methods Biomech. Biomed. Eng. 9, 371–377. doi:10.1080/10255840601003551.

Drapaca, C.S., Tenti, G., Rohlf, K., Sivaloganathan, S., 2006. A quasi-linear viscoelastic constitutive equation for the brain: application to hydrocephalus. J. Elast. 85, 65–83. doi:10.1007/s10659-006-9071-3.

Etoh, A., Mitaku, S., Yamamoto, J., Okano, K., 1994. Ultrasonic absorption anomaly of brain tissue. Jpn. J. Appl. Phys. 33, 2874–2879. doi:10.1143/JJAP.33.2874.

Fallah, A., Ahmadian, M.T., Firozbakhsh, K., Aghdam, M.M., 2017a. Micromechanical modeling of rate-dependent behavior of connective tissues. J. Theor. Biol. 416, 119–128. doi:10.1016/j.jtbi.2017.01.011.

Fallah, Ali, Ahmadian, M.T., Mohammadi Aghdam, M., 2017b. Rate-dependent behavior of connective tissue through a micromechanics-based hyper viscoelastic model. Int. J. Eng. Sci. 121, 91–107. doi:10.1016/j.ijengsci.2017.09.003.
Funk, J.R., Hall, G.W., Crandall, J.R., Pilkey, W.D., 2000. Linear and quasi-linear viscoelastic characterization of ankle ligaments. J. Biomech. Eng. 122, 15. doi:10.1115/1.429623.
Garcia-Gonzalez, D., Jérusalem, A., Garzon-Hernandez, S., Zaera, R., Arias, A., 2018. A continuum mechanics constitutive framework for transverse isotropic soft tissues. J. Mech. Phys. Solids 112, 209–224. doi:10.1016/j.jmps.2017.12.001.
Gent, A.N., 1996. A new constitutive relation for rubber. Rubber Chem. Technol. 69, 59–61. doi:10.5254/1.3538357.
Haldar, K., Pal, C., 2018. Rate dependent anisotropic constitutive modeling of brain tissue undergoing large deformation. J. Mech. Behav. Biomed. Mater. 81, 178–194. doi:10.1016/j.jmbbm.2017.12.021.
Harrigan, T.P., Roberts, J.C., Ward, E.E., Merkle, A.C., 2010. Correlating tissue response with anatomical location of mTBI using a human head finite element model under simulated blast conditions. In: IFMBE Proceedings, pp. 18–21. doi:10.1007/978-3-642-14998-6_5.
Holzapfel, G.A., Gasser, T.C., 2001. A viscoelastic model for fiber-reinforced composites at finite strains: continuum basis, computational aspects and applications. Comput. Methods Appl. Mech. Eng. 190, 4379–4403. doi:10.1016/S0045-7825(00)00323-6.
Hrapko, M., van Dommelen, J.A.W., Peters, G.W.M., Wismans, J.S.H.M., 2006. The mechanical behaviour of brain tissue: large strain response and constitutive modelling. Biorheology 43, 623–636.
Jennifer, M., Cronin, D.S., Worswick, M., Bourget, D., Williams, K., Pageau, G., 2001. Numerical modelling of a simplified surrogate leg subject to an anti-personnel blast mine. In: Proceedings of the 19th International Symposium of Ballistics, Interlaken, Switzerland, pp. 913–919.
Jiang, Y., Wang, Y., Peng, X., 2015. A visco-hyperelastic constitutive model for human spine ligaments. Cell Biochem. Biophys. 71, 1147–1156. doi:10.1007/s12013-014-0322-9.
Jin, X., Zhu, F., Mao, H., Shen, M., Yang, K.H., 2013. A comprehensive experimental study on material properties of human brain tissue. J. Biomech. 46, 2795–2801. doi:10.1016/j.jbiomech.2013.09.001.
Khajehsaeid, H., Arghavani, J., Naghdabadi, R., 2013. A hyperelastic constitutive model for rubber-like materials. Eur. J. Mech. - A/Solids 38, 144–151. doi:10.1016/j.euromechsol.2012.09.010.
Khajehsaeid, H., Arghavani, J., Naghdabadi, R., Sohrabpour, S., 2014. A visco-hyperelastic constitutive model for rubber-like materials: a rate-dependent relaxation time scheme. Int. J. Eng. Sci. 79, 44–58. doi:10.1016/j.ijengsci.2014.03.001.
Kulkarni, S.G., Gao, X.L., Horner, S.E., Mortlock, R.F., Zheng, J.Q., 2016. A transversely isotropic visco-hyperelastic constitutive model for soft tissues. Math. Mech. Solids 21, 747–770. doi:10.1177/1081286514536921.
Kwon, J., Subhash, G., 2010. Compressive strain rate sensitivity of ballistic gelatin. J. Biomech. 43, 420–425. doi:10.1016/j.jbiomech.2009.10.008.
Laiarinandrasana, L., Piques, R., Robisson, A., 2003. Visco-hyperelastic model with internal state variable coupled with discontinuous damage concept under total Lagrangian formulation. Int. J. Plast. 19, 977–1000. doi:10.1016/S0749-6419(02)00089-X.
Leclerc, G.E., Debernard, L., Foucart, F., Robert, L., Pelletier, K.M., Charleux, F., Ehman, R., Ho Ba Tho, M.C., Bensamoun, S.F., 2012. Characterization of a hyperviscoelastic phantom mimicking biological soft tissue using an abdominal pneumatic driver with magnetic resonance elastography (MRE). J. Biomech. 45, 952–957. doi:10.1016/j.jbiomech.2012.01.017.
Limbert, G., Middleton, J., 2004. A transversely isotropic viscohyperelastic material application to the modeling of biological soft connective tissues. Int. J. Solids Struct. 41, 4237–4260. doi:10.1016/j.ijsolstr.2004.02.057.
Lu, Y.T., Zhu, H.X., Richmond, S., Middleton, J., 2010. A visco-hyperelastic model for skeletal muscle tissue under high strain rates. J. Biomech. 43, 2629–2632. doi:10.1016/j.jbiomech.2010.05.030.
Luo, K., Upadhyay, K., Subhash, G., Spearot, D.E., 2019. Transient-State rheological behavior of poly(ethylene glycol) diacrylate hydrogels at high shear strain rates. Macromolecules 52, 5860–5871. doi:10.1021/acs.macromol.9b00820.
Mak, A.F., 1986. The apparent viscoelastic behavior of articular cartilage—the contributions from the intrinsic matrix viscoelasticity and interstitial fluid flows. J. Biomech. Eng. 108, 123. doi:10.1115/1.3138591.
Malvern, L.E., 1969. Introduction to the mechanics of a continuous medium. Prentice-Hall Series in Engineering of the Physical Sciences, 1st ed Prentice-Hall, Englewood Cliffs, USA.
Marckmann, G., Verron, E., 2006. Comparison of hyperelastic models for rubber-like materials. Rubber Chem. Technol. 79, 835–858. doi:10.5254/1.3547969.
McElhaney, J.H., Melvin, J.W., Roberts, V.L., Portnoy, H.D., 1973. Dynamic characteristics of the tissues of the head. In: Kenedi, R.M. (Ed.), Perspectives in Biomedical Engineering. Palgrave Macmillan, UK, London, pp. 215–222. doi:10.1007/978-1-349-01604-4_34.
Mihai, L.A., Budday, S., Holzapfel, G.A., Kuhl, E., Goriely, A., 2017. A family of hyperelastic models for human brain tissue. J. Mech. Phys. Solids 106, 60–79. doi:10.1016/j.jmps.2017.05.015.
Mohotti, D., Ali, M., Ngo, T., Lu, J., Mendis, P., 2014. Strain rate dependent constitutive model for predicting the material behaviour of polyurea under high strain rate tensile loading. Mater. Des. 53, 830–837. doi:10.1016/j.matdes.2013.07.020.
Mooney, M., 1940. A theory of large elastic deformation. J. Appl. Phys. 11, 582–592. doi:10.1063/1.1712836.
Naarayan, S.S., Subhash, G., 2017. Wave propagation in ballistic gelatine. J. Mech. Behav. Biomed. Mater. 68, 32–41. doi:10.1016/j.jmbbm.2017.01.030.
Naini, A.S., Patel, R.V., Samani, A., 2011. Measurement of lung hyperelastic properties using inverse finite element approach. IEEE Trans. Biomed. Eng. 58, 2852–2859. doi:10.1109/TBME.2011.2160637.
Nie, X., Song, B., Ge, Y., Chen, W.W., Weerasooriya, T., 2009. Dynamic tensile testing of soft materials. Exp. Mech. 49, 451–458. doi:10.1007/s11340-008-9133-5.
Ogden, R.W., 1972. Large deformation isotropic elasticity: on the correlation of theory and experiment for compressible rubberlike solids. Proc. R. Soc. A Math. Phys. Eng. Sci. 328, 567–583. doi:10.1098/rspa.1972.0096.
Ogden, R.W., Saccomandi, G., Sgura, I., 2004. Fitting hyperelastic models to experimental data. Comput. Mech. 34, 484–502. doi:10.1007/s00466-004-0593-y.
Parnaik, Y., Beillas, P., Demetropoulos, C.K., Hardy, W.N., Yang, K.H., King, A.I., 2004. The influence of surrogate blood vessels on the impact response of a physical model of the brain. Stapp Car Crash J. 48, 259–277.
Pavan, T.Z., Madsen, E.L., Frank, G.R., Adilton O Carneiro, A., Hall, T.J., 2010. Nonlinear elastic behavior of phantom materials for elastography. Phys. Med. Biol. 55, 2679–2692. doi:10.1088/0031-9155/55/9/017.
Payne, T., Mitchell, S., Bibb, R., Waters, M., 2015. The evaluation of new multi-material human soft tissue simulants for sports impact surrogates. J. Mech. Behav. Biomed. Mater. 41, 336–356. doi:10.1016/j.jmbbm.2014.09.018.
Pioletti, D.P., 2006. Viscoelastic constitutive law based on the time scale of the mechanical phenomena. In: Holzapfel, G.A., Ogden, R.W. (Eds.), Mechanics of Biological Tissue. Springer-Verlag, Berlin/ Heidelberg, pp. 399–404. doi:10.1007/3-540-31184-X_28.
Pioletti, D.P., Rakotomanana, L.R., 2000. Non-linear viscoelastic laws for soft biological tissues. Eur. J. Mech. - A/Solids 19, 749–759. doi:10.1016/S0997-7538(00)00202-3.
Pioletti, D.P., Rakotomanana, L.R., Benvenuti, J.F., Leyvraz, P.F., 1998. Viscoelastic constitutive law in large deformations: application to human knee ligaments and tendons. J. Biomech. 31, 753–757. doi:10.1016/S0021-9290(98)00077-3.
Prange, M.T., Margulies, S.S., 2002. Regional, directional, and age-dependent properties of the brain undergoing large deformation. J. Biomech. Eng. 124, 244. doi:10.1115/1.1449907.
Prange, M.T., Meaney, D.F., Margulies, S.S., 2000. Defining brain mechanical properties: effects of region, direction, and species. Stapp Car Crash J. 44, 205–213.
Pucci, E., Saccomandi, G., 2002. A note on the gent model for rubber-like materials. Rubber Chem. Technol. 75, 839–852. doi:10.5254/1.3547687.
Puglisi, G., Saccomandi, G., 2016. Multi-scale modelling of rubber-like materials and soft tissues: an appraisal. Proc. R. Soc. A Math. Phys. Eng. Sci. 472, 20160060. doi:10.1098/rspa.2016.0060.

Rashid, B., Destrade, M., Gilchrist, M.D., 2013. Mechanical characterization of brain tissue in simple shear at dynamic strain rates. J. Mech. Behav. Biomed. Mater. 28, 71–85. doi:10.1016/j.jmbbm.2013.07.017.
Reese, S., 2003. A micromechanically motivated material model for the thermo-viscoelastic material behaviour of rubber-like polymers. Int. J. Plast. 19, 909–940. doi:10.1016/S0749-6419(02)00086-4.
Reese, S., Govindjee, S., 1998. A theory of finite viscoelasticity and numerical aspects. Int. J. Solids Struct. 35, 3455–3482. doi:10.1016/S0020-7683(97)00217-5.
Rivlin, R.S., 1948a. Large elastic deformations of isotropic materials. IV. Further developments of the general theory. Philos. Trans. R. Soc. A Math. Phys. Eng. Sci. 241, 379–397. doi:10.1098/rsta.1948.0024.
Rivlin, R.S., 1948b. Large elastic deformations of isotropic materials. I. Fundamental concepts. Philos. Trans. R. Soc. A Math. Phys. Eng. Sci. 240, 459–490. doi:10.1098/rsta.1948.0002.
Roberts, J.C., Merkle, A.C., Biermann, P.J., Ward, E.E., Carkhuff, B.G., Cain, R.P., O'Connor, J.V., 2007. Computational and experimental models of the human torso for non-penetrating ballistic impact. J. Biomech. 40, 125–136. doi:10.1016/j.jbiomech.2005.11.003.
Sasso, M., Palmieri, G., Chiappini, G., Amodio, D., 2008. Characterization of hyperelastic rubber-like materials by biaxial and uniaxial stretching tests based on optical methods. Polym. Test. 27, 995–1004. doi:10.1016/j.polymertesting.2008.09.001.
Sasson, A., Patchornik, S., Eliasy, R., Robinson, D., Haj-Ali, R., 2012. Hyperelastic mechanical behavior of chitosan hydrogels for nucleus pulposus replacement-Experimental testing and constitutive modeling. J. Mech. Behav. Biomed. Mater. 8, 143–153. doi:10.1016/j.jmbbm.2011.12.008.
Shim, V.P.W., Yang, L.M., Lim, C.T., Law, P.H., 2004. A visco-hyperelastic constitutive model to characterize both tensile and compressive behavior of rubber. J. Appl. Polym. Sci. 92, 523–531. doi:10.1002/app.20029.
Simo, J.C., 1987. On a fully three-dimensional finite-strain viscoelastic damage model: formulation and computational aspects. Comput. Methods Appl. Mech. Eng. 60, 153–173. doi:10.1016/0045-7825(87)90107-1.
Siviour, C.R., Jordan, J.L., 2016. High strain rate mechanics of polymers: a review. J. Dyn. Behav. Mater. 2, 15–32. doi:10.1007/s40870-016-0052-8.
Chafi, Sotudeh, M., Karami, G., Ziejewski, 2007. Simulation of blast-head interactions to study traumatic brain injury. In: Volume 2: Biomedical and Biotechnology Engineering. ASME, pp. 211–220. doi:10.1115/IMECE2007-41629.
Subhash, G., Kwon, J., Mei, R., Moore, D.F., 2012. Non-Newtonian behavior of ballistic gelatin at high shear rates. Exp. Mech. 52, 551–560. doi:10.1007/s11340-011-9513-0.
Svensson, R.B., Hassenkam, T., Hansen, P., Magnusson, Peter, 2010. Viscoelastic behavior of discrete human collagen fibrils. J. Mech. Behav. Biomed. Mater. 3, 112–115. doi:10.1016/j.jmbbm.2009.01.005.
Tian, W., Hou, S.P., Ma, J., Zhang, C., Xu, Q.Y., Lee, I.S., Li, H.D., Spector, M., Cui, F.Z., 2005. Hyaluronic acid–poly-D-lysine-based three-dimensional hydrogel for traumatic brain injury. Tissue Eng. 11, 513–525. doi:10.1089/ten.2005.11.513.
Treloar, L.R.G., 1944. The elasticity of a network of long-chain molecules. II. Rubber Chem. Technol. 17, 296–302. doi:10.5254/1.3546653.
Upadhyay, K., Bhattacharyya, A., Subhash, G., Spearot, D.E., 2019a. Quasi-static and high strain rate simple shear characterization of soft polymers. Exp. Mech. 59, 733–747. doi:10.1007/s11340-019-00507-1.
Upadhyay, K., Subhash, G., Spearot, D., 2019b. Thermodynamics-based stability criteria for constitutive equations of isotropic hyperelastic solids. J. Mech. Phys. Solids 124, 115–142. doi:10.1016/j.jmps.2018.09.038.
van Dommelen, J.A.W., Hrapko, M., Peters, G.W.M., 2009. Mechanical properties of brain tissue: characterisation and constitutive modelling. In: Mechanosensitivity of the Nervous System. Springer, Netherlands, Dordrecht, pp. 249–279. doi:10.1007/978-1-4020-8716-5_12.
Vogel, A., Rakotomanana, L., Pioletti, D.P., 2017. Viscohyperelastic strain energy function. In: Biomechanics of Living Organs. Elsevier, pp. 59–78. doi:10.1016/B978-0-12-804009-6.00003-1.
Wex, C., Arndt, S., Stoll, A., Bruns, C., Kupriyanova, Y., 2015. Isotropic incompressible hyperelastic models for modelling the mechanical behaviour of biological tissues: a review. Biomed. Eng. / Biomed. Tech. 60, 577–592. doi:10.1515/bmt-2014-0146.
Xiang, Y., Zhong, D., Wang, P., Yin, T., Zhou, H., Yu, H., Baliga, C., Qu, S., Yang, W., 2019. A physically based visco-hyperelastic constitutive model for soft materials. J. Mech. Phys. Solids 128, 208–218. doi:10.1016/j.jmps.2019.04.010.
Yang, L.M., Shim, V.P.W., Lim, C.T., 2000. A visco-hyperelastic approach to modelling the constitutive behaviour of rubber. Int. J. Impact Eng. 24, 545–560. doi:10.1016/S0734-743X(99)00044-5.
Yousefi, A.A.K., Nazari, M.A., Perrier, P., Panahi, M.S., Payan, Y., 2018. A visco-hyperelastic constitutive model and its application in bovine tongue tissue. J. Biomech. 71, 190–198. doi:10.1016/j.jbiomech.2018.02.008.
Zhang, J., Yoganandan, N., Pintar, F.A., Gennarelli, T.A., 2005. Temporal cavity and pressure distribution in a brain simulant following ballistic penetration. J. Neurotrauma 22, 1335–1347. doi:10.1089/neu.2005.22.1335.
Zhao, W., Shi, Z., Chen, X., Yang, G., Lenardi, C., Liu, C., 2015. Microstructural and mechanical characteristics of PHEMA-based nanofibre-reinforced hydrogel under compression. Compos. Part B Eng. 76, 292–299. doi:10.1016/j.compositesb.2015.02.033.
Zhong, H., Peters, T., 2007. A real time hyperelastic tissue model. Comput. Methods Biomech. Biomed. Eng. 10, 185–193. doi:10.1080/10255840701292732.
Zhurov, A.I., Limbert, G., Aeschlimann, D.P., Middleton, J., 2007. A constitutive model for the periodontal ligament as a compressible transversely isotropic visco-hyperelastic tissue. Comput. Methods Biomech. Biomed. Eng. 10, 223–235. doi:10.1080/13639080701314894.

Kshitiz Upadhyay is a PhD candidate in the Mechanical and Aerospace Engineering department at the University of Florida, where he also serves as a graduate research assistant in the Laboratory for Dynamic Response of Advanced Materials (LDRAM). His research focus is twofold: to design novel experiments for characterizing soft materials in a wide range of deformation modes and loading rates, and to develop rate-sensitive constitutive relations and numerical simulations for modeling their mechanical response. He has published 1 book chapter and 4 journal papers in reputed international journals. He was recently awarded the 2019 Outstanding International Student Award from the University of Florida, first place at the 2019 SEM Michael Sutton International Student paper Competition and 2019 SMARTS Symposium. He holds a Master of Science in Mechanical Engineering from the University of Florida, and a Bachelor of Technology in Mechanical Engineering from the National Institute of Technology, Bhopal, India.

Ghatu Subhash is the Newton C. Ebaugh Professor in the Department of Mechanical and Aerospace Engineering at the University of Florida. His research expertise is in the broad area of solid mechanics with emphasis on multiaxial constitutive response of advanced materials, high strain rate behavior, experimental solid mechanics and process-structure relationships. He is a fellow of ASME and SEM. He currently serves as the editor-in-chief of *Mechanics of Materials*, and an associate editor of *J Am Cer Soc* and *J Eng Mater Tech*. He has recently received M.M Frocht Award from *Exp Mech*, ORR Best Paper Award from *J Eng Mater Tech* and 'Significant Contribution Award' from the American Nuclear Society.

Douglas Spearot is an Associate Professor in the Department of Mechanical & Aerospace Engineering at the University of Florida. His research focuses on the use of atomistic and mesoscale simulation techniques to study the mechanical and thermodynamic properties of materials. Dr. Spearot was awarded the NSF CAREER Award to elucidate the nanoscale mechanisms associated with phase nucleation during physical vapor deposition. Dr. Spearot received his Bachelor of Science in Mechanical Engineering from the University of Michigan. He completed his Master of Science and Ph.D. degrees in Mechanical Engineering from the Georgia Institute of Technology.